Syracuse University
SURFACE

Physics | College of Arts and Sciences

9-30-2011

Measurements of the Branching Fractions for B_(s) -> D_(s)πππ and Λ_b^0 -> Λ_c^+πππ

Raymond Mountain
Syracuse University

Marina Artuso
Syracuse University

S. Blusk
Syracuse University

Alessandra Borgia
Syracuse University

Follow this and additional works at: http://surface.syr.edu/phy

Part of the Physics Commons

Repository Citation
Mountain, Raymond; Artuso, Marina; Blusk, S.; and Borgia, Alessandra, "Measurements of the Branching Fractions for B_(s) -> D_(s)πππ and Λ_b^0 -> Λ_c^+πππ" (2011). *Physics.* Paper 368.
http://surface.syr.edu/phy/368

This Article is brought to you for free and open access by the College of Arts and Sciences at SURFACE. It has been accepted for inclusion in Physics by an authorized administrator of SURFACE. For more information, please contact surface@syr.edu.

EUROPEAN ORGANIZATION FOR NUCLEAR RESEARCH (CERN)

LHCb-PAPER-2011-016
CERN-PH-EP-2011-151
October 3, 2011

arXiv:1109.6831v1 [hep-ex] 30 Sep 2011

Measurements of the Branching fractions for $B_{(s)} \to D_{(s)}\pi\pi\pi$ and $\Lambda_b^0 \to \Lambda_c^+\pi\pi\pi$

The LHCb Collaboration [1]

Abstract

Branching fractions of the decays $H_b \to H_c\pi^-\pi^+\pi^-$ relative to $H_b \to H_c\pi^-$ are presented, where H_b (H_c) represents $\bar{B}^0$ (D^+), B^- (D^0), $\bar{B}_s^0$ (D_s^+) and Λ_b^0 (Λ_c^+). The measurements are performed with the LHCb detector using 35 pb^{-1} of data collected at $\sqrt{s} = 7$ TeV. The ratios of branching fractions are measured to be

$$\frac{\mathcal{B}(\overline{B}^0 \to D^+\pi^-\pi^+\pi^-)}{\mathcal{B}(\overline{B}^0 \to D^+\pi^-)} = 2.38 \pm 0.11 \pm 0.21$$
$$\frac{\mathcal{B}(B^- \to D^0\pi^-\pi^+\pi^-)}{\mathcal{B}(B^- \to D^0\pi^-)} = 1.27 \pm 0.06 \pm 0.11$$
$$\frac{\mathcal{B}(\overline{B}_s^0 \to D_s^+\pi^-\pi^+\pi^-)}{\mathcal{B}(\overline{B}_s^0 \to D_s^+\pi^-)} = 2.01 \pm 0.37 \pm 0.20$$
$$\frac{\mathcal{B}(\Lambda_b^0 \to \Lambda_c^+\pi^-\pi^+\pi^-)}{\mathcal{B}(\Lambda_b^0 \to \Lambda_c^+\pi^-)} = 1.43 \pm 0.16 \pm 0.13.$$

We also report measurements of partial decay rates of these decays to excited charm hadrons. These results are of comparable or higher precision than existing measurements.

[1] Authors are listed on the following pages.

R. Aaij[23], B. Adeva[36], M. Adinolfi[42], C. Adrover[6], A. Affolder[48], Z. Ajaltouni[5], J. Albrecht[37], F. Alessio[37], M. Alexander[47], G. Alkhazov[29], P. Alvarez Cartelle[36], A.A. Alves Jr[22], S. Amato[2], Y. Amhis[38], J. Anderson[39], R.B. Appleby[50], O. Aquines Gutierrez[10], F. Archilli[18,37], L. Arrabito[53], A. Artamonov [34], M. Artuso[52,37], E. Aslanides[6], G. Auriemma[22,m], S. Bachmann[11], J.J. Back[44], D.S. Bailey[50], V. Balagura[30,37], W. Baldini[16], R.J. Barlow[50], C. Barschel[37], S. Barsuk[7], W. Barter[43], A. Bates[47], C. Bauer[10], Th. Bauer[23], A. Bay[38], I. Bediaga[1], K. Belous[34], I. Belyaev[30,37], E. Ben-Haim[8], M. Benayoun[8], G. Bencivenni[18], S. Benson[46], J. Benton[42], R. Bernet[39], M.-O. Bettler[17], M. van Beuzekom[23], A. Bien[11], S. Bifani[12], A. Bizzeti[17,h], P.M. Bjørnstad[50], T. Blake[49], F. Blanc[38], C. Blanks[49], J. Blouw[11], S. Blusk[52], A. Bobrov[33], V. Bocci[22], A. Bondar[33], N. Bondar[29], W. Bonivento[15], S. Borghi[47], A. Borgia[52], T.J.V. Bowcock[48], C. Bozzi[16], T. Brambach[9], J. van den Brand[24], J. Bressieux[38], D. Brett[50], S. Brisbane[51], M. Britsch[10], T. Britton[52], N.H. Brook[42], H. Brown[48], A. Büchler-Germann[39], I. Burducea[28], A. Bursche[39], J. Buytaert[37], S. Cadeddu[15], J.M. Caicedo Carvajal[37], O. Callot[7], M. Calvi[20,j], M. Calvo Gomez[35,n], A. Camboni[35], P. Campana[18,37], A. Carbone[14], G. Carboni[21,k], R. Cardinale[19,i,37], A. Cardini[15], L. Carson[36], K. Carvalho Akiba[23], G. Casse[48], M. Cattaneo[37], M. Charles[51], Ph. Charpentier[37], N. Chiapolini[39], K. Ciba[37], X. Cid Vidal[36], G. Ciezarek[49], P.E.L. Clarke[46,37], M. Clemencic[37], H.V. Cliff[43], J. Closier[37], C. Coca[28], V. Coco[23], J. Cogan[6], P. Collins[37], F. Constantin[28], G. Conti[38], A. Contu[51], A. Cook[42], M. Coombes[42], G. Corti[37], G.A. Cowan[38], R. Currie[46], B. D'Almagne[7], C. D'Ambrosio[37], P. David[8], I. De Bonis[4], S. De Capua[21,k], M. De Cian[39], F. De Lorenzi[12], J.M. De Miranda[1], L. De Paula[2], P. De Simone[18], D. Decamp[4], M. Deckenhoff[9], H. Degaudenzi[38,37], M. Deissenroth[11], L. Del Buono[8], C. Deplano[15], O. Deschamps[5], F. Dettori[15,d], J. Dickens[43], H. Dijkstra[37], P. Diniz Batista[1], S. Donleavy[48], A. Dosil Suárez[36], D. Dossett[44], A. Dovbnya[40], F. Dupertuis[38], R. Dzhelyadin[34], C. Eames[49], S. Easo[45], U. Egede[49], V. Egorychev[30], S. Eidelman[33], D. van Eijk[23], F. Eisele[11], S. Eisenhardt[46], R. Ekelhof[9], L. Eklund[47], Ch. Elsasser[39], D.G. d'Enterria[35,o], D. Esperante Pereira[36], L. Estève[43], A. Falabella[16,e], E. Fanchini[20,j], C. Färber[11], G. Fardell[46], C. Farinelli[23], S. Farry[12], V. Fave[38], V. Fernandez Albor[36], M. Ferro-Luzzi[37], S. Filippov[32], C. Fitzpatrick[46], M. Fontana[10], F. Fontanelli[19,i], R. Forty[37], M. Frank[37], C. Frei[37], M. Frosini[17,f,37], S. Furcas[20], A. Gallas Torreira[36], D. Galli[14,c], M. Gandelman[2], P. Gandini[51], Y. Gao[3], J-C. Garnier[37], J. Garofoli[52], J. Garra Tico[43], L. Garrido[35], C. Gaspar[37], N. Gauvin[38], M. Gersabeck[37], T. Gershon[44,37], Ph. Ghez[4], V. Gibson[43], V.V. Gligorov[37], C. Göbel[54], D. Golubkov[30], A. Golutvin[49,30,37], A. Gomes[2], H. Gordon[51], M. Grabalosa Gándara[35], R. Graciani Diaz[35], L.A. Granado Cardoso[37], E. Graugés[35], G. Graziani[17], A. Grecu[28], S. Gregson[43], B. Gui[52], E. Gushchin[32], Yu. Guz[34], T. Gys[37], G. Haefeli[38], C. Haen[37], S.C. Haines[43], T. Hampson[42], S. Hansmann-Menzemer[11], R. Harji[49], N. Harnew[51], J. Harrison[50], P.F. Harrison[44], J. He[7], V. Heijne[23], K. Hennessy[48], P. Henrard[5], J.A. Hernando Morata[36], E. van Herwijnen[37], E. Hicks[48], W. Hofmann[10], K. Holubyev[11], P. Hopchev[4], W. Hulsbergen[23], P. Hunt[51], T. Huse[48], R.S. Huston[12], D. Hutchcroft[48], D. Hynds[47], V. Iakovenko[41], P. Ilten[12], J. Imong[42], R. Jacobsson[37], A. Jaeger[11], M. Jahjah Hussein[5], E. Jans[23], F. Jansen[23], P. Jaton[38], B. Jean-Marie[7], F. Jing[3], M. John[51], D. Johnson[51], C.R. Jones[43], B. Jost[37], S. Kandybei[40], M. Karacson[37], T.M. Karbach[9], J. Keaveney[12], U. Kerzel[37], T. Ketel[24], A. Keune[38], B. Khanji[6], Y.M. Kim[46], M. Knecht[38], S. Koblitz[37], P. Koppenburg[23], A. Kozlinskiy[23], L. Kravchuk[32], K. Kreplin[11], M. Kreps[44], G. Krocker[11], P. Krokovny[11], F. Kruse[9], K. Kruzelecki[37], M. Kucharczyk[20,25,37], S. Kukulak[25], R. Kumar[14,37], T. Kvaratskheliya[30,37], V.N. La Thi[38], D. Lacarrere[37], G. Lafferty[50], A. Lai[15], D. Lambert[46], R.W. Lambert[37], E. Lanciotti[37], G. Lanfranchi[18], C. Langenbruch[11], T. Latham[44], R. Le Gac[6], J. van Leerdam[23], J.-P. Lees[4], R. Lefèvre[5], A. Leflat[31,37], J. Lefrançois[7], O. Leroy[6], T. Lesiak[25], L. Li[3], L. Li Gioi[5], M. Lieng[9], M. Liles[48], R. Lindner[37], C. Linn[11], B. Liu[3], G. Liu[37], J.H. Lopes[2], E. Lopez Asamar[35], N. Lopez-March[38], J. Luisier[38], F. Machefert[7], I.V. Machikhiliyan[4,30], F. Maciuc[10], O. Maev[29,37], J. Magnin[1], S. Malde[51], R.M.D. Mamunur[37], G. Manca[15,d], G. Mancinelli[6], N. Mangiafave[43], U. Marconi[14], R. Märki[38], J. Marks[11], G. Martellotti[22], A. Martens[7], L. Martin[51], A. Martín Sánchez[7], D. Martinez Santos[37], A. Massafferri[1], Z. Mathe[12], C. Matteuzzi[20], M. Matveev[29], E. Maurice[6], B. Maynard[52], A. Mazurov[32,16,37], G. McGregor[50], R. McNulty[12], C. Mclean[14], M. Meissner[11], M. Merk[23], J. Merkel[9], R. Messi[21,k], S. Miglioranzi[37], D.A. Milanes[13,37], M.-N. Minard[4], S. Monteil[5], D. Moran[12], P. Morawski[25], R. Mountain[52], I. Mous[23], F. Muheim[46], K. Müller[39], R. Muresan[28,38], B. Muryn[26], M. Musy[35], J. Mylroie-Smith[48], P. Naik[42],

T. Nakada[38], R. Nandakumar[45], J. Nardulli[45], I. Nasteva[1], M. Nedos[9], M. Needham[46], N. Neufeld[37], C. Nguyen-Mau[38,p], M. Nicol[7], S. Nies[9], V. Niess[5], N. Nikitin[31], A. Oblakowska-Mucha[26], V. Obraztsov[34], S. Oggero[23], S. Ogilvy[47], O. Okhrimenko[41], R. Oldeman[15,d], M. Orlandea[28], J.M. Otalora Goicochea[2], P. Owen[49], B. Pal[52], J. Palacios[39], M. Palutan[18], J. Panman[37], A. Papanestis[45], M. Pappagallo[13,b], C. Parkes[47,37], C.J. Parkinson[49], G. Passaleva[17], G.D. Patel[48], M. Patel[49], S.K. Paterson[49], G.N. Patrick[45], C. Patrignani[19,i], C. Pavel-Nicorescu[28], A. Pazos Alvarez[36], A. Pellegrino[23], G. Penso[22,l], M. Pepe Altarelli[37], S. Perazzini[14,c], D.L. Perego[20,j], E. Perez Trigo[36], A. Pérez-Calero Yzquierdo[35], P. Perret[5], M. Perrin-Terrin[6], G. Pessina[20], A. Petrella[16,37], A. Petrolini[19,i], B. Pie Valls[35], B. Pietrzyk[4], T. Pilar[44], D. Pinci[22], R. Plackett[47], S. Playfer[46], M. Plo Casasus[36], G. Polok[25], A. Poluektov[44,33], E. Polycarpo[2], D. Popov[10], B. Popovici[28], C. Potterat[35], A. Powell[51], T. du Pree[23], J. Prisciandaro[38], V. Pugatch[41], A. Puig Navarro[35], W. Qian[52], J.H. Rademacker[42], B. Rakotomiaramanana[38], M.S. Rangel[2], I. Raniuk[40], G. Raven[24], S. Redford[51], M.M. Reid[44], A.C. dos Reis[1], S. Ricciardi[45], K. Rinnert[48], D.A. Roa Romero[5], P. Robbe[7], E. Rodrigues[47], F. Rodrigues[2], P. Rodriguez Perez[36], G.J. Rogers[43], S. Roiser[37], V. Romanovsky[34], J. Rouvinet[38], T. Ruf[37], H. Ruiz[35], G. Sabatino[21,k], J.J. Saborido Silva[36], N. Sagidova[29], P. Sail[47], B. Saitta[15,d], C. Salzmann[39], M. Sannino[19,i], R. Santacesaria[22], R. Santinelli[37], E. Santovetti[21,k], M. Sapunov[6], A. Sarti[18,l], C. Satriano[22,m], A. Satta[21], M. Savrie[16,e], D. Savrina[30], P. Schaack[49], M. Schiller[11], S. Schleich[9], M. Schmelling[10], B. Schmidt[37], O. Schneider[38], A. Schopper[37], M.-H. Schune[7], R. Schwemmer[37], A. Sciubba[18,l], M. Seco[36], A. Semennikov[30], K. Senderowska[26], I. Sepp[49], N. Serra[39], J. Serrano[6], P. Seyfert[11], B. Shao[3], M. Shapkin[34], I. Shapoval[40,37], P. Shatalov[30], Y. Shcheglov[29], T. Shears[48], L. Shekhtman[33], O. Shevchenko[40], V. Shevchenko[30], A. Shires[49], R. Silva Coutinho[54], H.P. Skottowe[43], T. Skwarnicki[52], A.C. Smith[37], N.A. Smith[48], K. Sobczak[5], F.J.P. Soler[47], A. Solomin[42], F. Soomro[49], B. Souza De Paula[2], B. Spaan[9], A. Sparkes[46], P. Spradlin[47], F. Stagni[37], S. Stahl[11], O. Steinkamp[39], S. Stoica[28], S. Stone[52,37], B. Storaci[23], M. Straticiuc[28], U. Straumann[39], N. Styles[46], V.K. Subbiah[37], S. Swientek[9], M. Szczekowski[27], P. Szczypka[38], T. Szumlak[26], S. T'Jampens[4], E. Teodorescu[28], F. Teubert[37], C. Thomas[51,45], E. Thomas[37], J. van Tilburg[11], V. Tisserand[4], M. Tobin[39], S. Topp-Joergensen[51], M.T. Tran[38], A. Tsaregorodtsev[6], N. Tuning[23], A. Ukleja[27], P. Urquijo[52], U. Uwer[11], V. Vagnoni[14], G. Valenti[14], R. Vazquez Gomez[35], P. Vazquez Regueiro[36], S. Vecchi[16], J.J. Velthuis[42], M. Veltri[17,g], K. Vervink[37], B. Viaud[7], I. Videau[7], X. Vilasis-Cardona[35,n], J. Visniakov[36], A. Vollhardt[39], D. Voong[42], A. Vorobyev[29], H. Voss[10], K. Wacker[9], S. Wandernoth[11], J. Wang[52], D.R. Ward[43], A.D. Webber[50], D. Websdale[49], M. Whitehead[44], D. Wiedner[11], L. Wiggers[23], G. Wilkinson[51], M.P. Williams[44,45], M. Williams[49], F.F. Wilson[45], J. Wishahi[9], M. Witek[25,37], W. Witzeling[37], S.A. Wotton[43], K. Wyllie[37], Y. Xie[46], F. Xing[51], Z. Yang[3], R. Young[46], O. Yushchenko[34], M. Zavertyaev[10,a], L. Zhang[52], W.C. Zhang[12], Y. Zhang[3], A. Zhelezov[11], L. Zhong[3], E. Zverev[31], A. Zvyagin [37].

[1] *Centro Brasileiro de Pesquisas Físicas (CBPF), Rio de Janeiro, Brazil*

[2] *Universidade Federal do Rio de Janeiro (UFRJ), Rio de Janeiro, Brazil*

[3] *Center for High Energy Physics, Tsinghua University, Beijing, China*

[4] *LAPP, Université de Savoie, CNRS/IN2P3, Annecy-Le-Vieux, France*

[5] *Clermont Université, Université Blaise Pascal, CNRS/IN2P3, LPC, Clermont-Ferrand, France*

[6] *CPPM, Aix-Marseille Université, CNRS/IN2P3, Marseille, France*

[7] *LAL, Université Paris-Sud, CNRS/IN2P3, Orsay, France*

[8] *LPNHE, Université Pierre et Marie Curie, Université Paris Diderot, CNRS/IN2P3, Paris, France*

[9] *Fakultät Physik, Technische Universität Dortmund, Dortmund, Germany*

[10] *Max-Planck-Institut für Kernphysik (MPIK), Heidelberg, Germany*

[11] *Physikalisches Institut, Ruprecht-Karls-Universität Heidelberg, Heidelberg, Germany*

[12] *School of Physics, University College Dublin, Dublin, Ireland*

[13] *Sezione INFN di Bari, Bari, Italy*

[14] *Sezione INFN di Bologna, Bologna, Italy*

[15] *Sezione INFN di Cagliari, Cagliari, Italy*
[16] *Sezione INFN di Ferrara, Ferrara, Italy*
[17] *Sezione INFN di Firenze, Firenze, Italy*
[18] *Laboratori Nazionali dell'INFN di Frascati, Frascati, Italy*
[19] *Sezione INFN di Genova, Genova, Italy*
[20] *Sezione INFN di Milano Bicocca, Milano, Italy*
[21] *Sezione INFN di Roma Tor Vergata, Roma, Italy*
[22] *Sezione INFN di Roma La Sapienza, Roma, Italy*
[23] *Nikhef National Institute for Subatomic Physics, Amsterdam, Netherlands*
[24] *Nikhef National Institute for Subatomic Physics and Vrije Universiteit, Amsterdam, Netherlands*
[25] *Henryk Niewodniczanski Institute of Nuclear Physics Polish Academy of Sciences, Cracow, Poland*
[26] *Faculty of Physics & Applied Computer Science, Cracow, Poland*
[27] *Soltan Institute for Nuclear Studies, Warsaw, Poland*
[28] *Horia Hulubei National Institute of Physics and Nuclear Engineering, Bucharest-Magurele, Romania*
[29] *Petersburg Nuclear Physics Institute (PNPI), Gatchina, Russia*
[30] *Institute of Theoretical and Experimental Physics (ITEP), Moscow, Russia*
[31] *Institute of Nuclear Physics, Moscow State University (SINP MSU), Moscow, Russia*
[32] *Institute for Nuclear Research of the Russian Academy of Sciences (INR RAN), Moscow, Russia*
[33] *Budker Institute of Nuclear Physics (SB RAS) and Novosibirsk State University, Novosibirsk, Russia*
[34] *Institute for High Energy Physics (IHEP), Protvino, Russia*
[35] *Universitat de Barcelona, Barcelona, Spain*
[36] *Universidad de Santiago de Compostela, Santiago de Compostela, Spain*
[37] *European Organization for Nuclear Research (CERN), Geneva, Switzerland*
[38] *Ecole Polytechnique Fédérale de Lausanne (EPFL), Lausanne, Switzerland*
[39] *Physik-Institut, Universität Zürich, Zürich, Switzerland*
[40] *NSC Kharkiv Institute of Physics and Technology (NSC KIPT), Kharkiv, Ukraine*
[41] *Institute for Nuclear Research of the National Academy of Sciences (KINR), Kyiv, Ukraine*
[42] *H.H. Wills Physics Laboratory, University of Bristol, Bristol, United Kingdom*
[43] *Cavendish Laboratory, University of Cambridge, Cambridge, United Kingdom*
[44] *Department of Physics, University of Warwick, Coventry, United Kingdom*
[45] *STFC Rutherford Appleton Laboratory, Didcot, United Kingdom*
[46] *School of Physics and Astronomy, University of Edinburgh, Edinburgh, United Kingdom*
[47] *School of Physics and Astronomy, University of Glasgow, Glasgow, United Kingdom*
[48] *Oliver Lodge Laboratory, University of Liverpool, Liverpool, United Kingdom*
[49] *Imperial College London, London, United Kingdom*
[50] *School of Physics and Astronomy, University of Manchester, Manchester, United Kingdom*
[51] *Department of Physics, University of Oxford, Oxford, United Kingdom*
[52] *Syracuse University, Syracuse, NY, United States*
[53] *CC-IN2P3, CNRS/IN2P3, Lyon-Villeurbanne, France, associated member*
[54] *Pontifícia Universidade Católica do Rio de Janeiro (PUC-Rio), Rio de Janeiro, Brazil, associated to* [2]

[a] *P.N. Lebedev Physical Institute, Russian Academy of Science (LPI RAS), Moscow, Russia*
[b] *Università di Bari, Bari, Italy*

[c] *Università di Bologna, Bologna, Italy*
[d] *Università di Cagliari, Cagliari, Italy*
[e] *Università di Ferrara, Ferrara, Italy*
[f] *Università di Firenze, Firenze, Italy*
[g] *Università di Urbino, Urbino, Italy*
[h] *Università di Modena e Reggio Emilia, Modena, Italy*
[i] *Università di Genova, Genova, Italy*
[j] *Università di Milano Bicocca, Milano, Italy*
[k] *Università di Roma Tor Vergata, Roma, Italy*
[l] *Università di Roma La Sapienza, Roma, Italy*
[m] *Università della Basilicata, Potenza, Italy*
[n] *LIFAELS, La Salle, Universitat Ramon Llull, Barcelona, Spain*
[o] *Institució Catalana de Recerca i Estudis Avançats (ICREA), Barcelona, Spain*
[p] *Hanoi University of Science, Hanoi, Viet Nam*

1 Introduction

Over the last two decades, a wealth of information has been accumulated on the decays of b-hadrons. Measurements of their decays have been used to test the CKM mechanism [1] for describing weak decay phenomena in the Standard Model, as well as provide measurements against which various theoretical approaches, such as HQET [2] and the factorization hypothesis, can be compared. While many decays have been measured, a large number remain either unobserved or poorly measured, most notably in the decays of B_s^0 mesons and Λ_b^0 baryons. Among the largest hadronic branching fractions are the decays $H_b \to H_c\pi^-\pi^+\pi^-$, where H_b (H_c) represents $\overline{B}^0$ (D^+), B^- (D^0), $\overline{B}_s^0$ (D_s^+) and Λ_b^0 (Λ_c^+). The first three branching fractions were determined with only 30-40% accuracy, and the $\Lambda_b^0 \to \Lambda_c^+\pi^-\pi^+\pi^-$ branching fraction was unmeasured.

Beyond improving our overall understanding of hadronic b decays, these decays are of interest because of their potential use in CP violation studies. It is well known that the Cabibbo-suppressed decays $B^- \to DK^-$ [3, 4, 5] and $\overline{B}_s^0 \to D_s^\pm K^\mp$ [6, 7] provide clean measurements of the weak phase γ through time-independent and time-dependent rate measurements, respectively. Additional sensitivity can be obtained by using $\overline{B}^0 \to D^+\pi^-$ [8] decays. As well as these modes, one can exploit higher multiplicity decays, such as $\overline{B}^0 \to DK^{*0}$, $B^- \to DK^-\pi^+\pi^-$ [9] and $\overline{B}_s^0 \to D_s^\pm K^\mp\pi^\pm\pi^\mp$. Moreover, the decay $\overline{B}_s^0 \to D_s^+\pi^-\pi^+\pi^-$ has been used to measure Δm_s [10], and with a sufficiently large sample, provides a calibration for the flavor-mistag rate for the time-dependent analysis of $\overline{B}_s^0 \to D_s^\pm K^\mp\pi^\pm\pi^\mp$.

The first step towards exploiting these multi-body decays is to observe them and quantify their branching fractions. The more interesting Cabibbo-suppressed decays are $O(\lambda^3)$ in the Wolfenstein parameterization [11], and therefore require larger data samples. Here, we present measurements of the Cabibbo-favored $H_b \to H_c\pi^-\pi^+\pi^-$ decays. The leading amplitudes contributing to these final states are shown in Fig. 1. Additional contributions from annihilation and W-exchange diagrams are suppressed and are not shown here. Note that for the B^- and Λ_b^0 decays, unlike the $\overline{B}^0$ and $\overline{B}_s^0$, there is potential for interference between diagrams with similar magnitudes. In Ref. [12], it is argued that this interference can explain the larger rate for $B^- \to D^0\pi^-$ compared to $\overline{B}^0 \to D^+\pi^-$. Thus, it is interesting to see whether this is also true when the final state contains three pions.

In this paper, we report measurements of the $H_b \to H_c\pi^-\pi^+\pi^-$ branching fractions, relative to $H_b \to H_c\pi^-$. We also report on the partial branching fractions, $H_b \to H_c^*\pi^-$, $H_c^* \to H_c\pi^+\pi^-$, where H_b is either $\overline{B}^0$, B^-, or Λ_b^0, and H_c^* refers to $D_1(2420)^{+,0}$, $D_2^*(2460)^0$, $\Lambda_c(2595)^+$, or $\Lambda_c(2625)^+$. We also present results on the partial rates for $\Lambda_b^0 \to \Sigma_c(2544)^{0,++}\pi^\pm\pi^-$. Charge conjugate final states are implied throughout.

2 Detector and Trigger

The data used for this analysis were collected by the LHCb experiment during the 2010 data taking period and comprise about 35 pb^{-1} of integrated luminosity. LHCb has

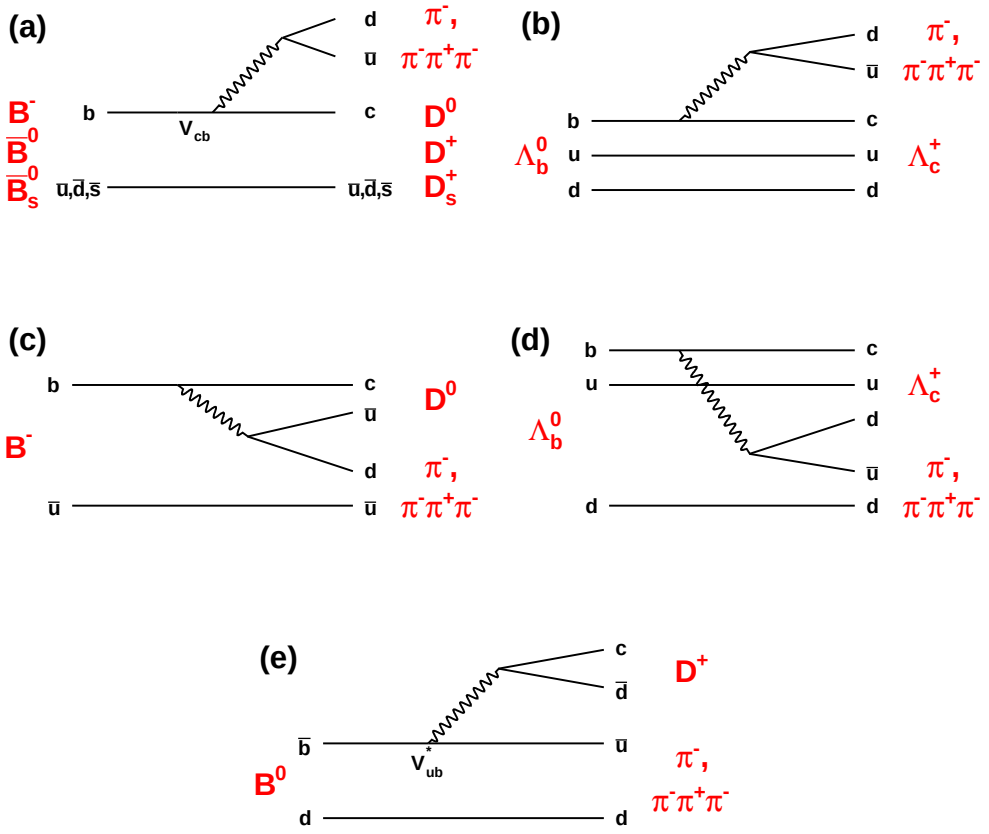

Figure 1: Feynman diagrams for $H_b \to H_c\pi^-$ and $H_b \to H_c\pi^-\pi^+\pi^-$ decays. Figs. (a) and (b) show external tree diagrams, (c) and (d) show color-suppressed tree diagrams (B^- and Λ_b^0 only), and (e) shows the Cabibbo-suppressed external tree diagram, only accessible to B^0 meson.

excellent capabilities to trigger on and reconstruct bottom and charm hadrons. The most important element of the detector for this analysis is a charged particle tracking system that covers the forward angular region from about $15 - 350$ mrad and $15 - 250$ mrad in the horizontal and vertical directions, respectively. It includes a 21 station, one-meter long array of silicon strip detectors (VELO) that come within 8 mm of the LHC beams, a 4 Tm dipole magnetic field, followed by three multi-layer tracking stations (T-stations) downstream of the dipole magnet. Each T-station is composed of a four layer silicon strip detector (IT) in the high occupancy region near the beam pipe, an eight layer straw tube drift chamber (OT) composed of 5 mm diameter straws outside this high occupancy region. Just upstream of the dipole magnet is a four-layer silicon strip detector (TT). Overall, the tracking system provides an impact parameter (IP) resolution of $\sim 16\mu$m $+$ 30μm$/p_T$ (transverse momentum, p_T in GeV$/c$), and a momentum resolution that ranges from $\sigma_p/p \sim 0.4\%$ at 3 GeV$/c$ to $\sim 0.6\%$ at 100 GeV$/c$. Two Ring Imaging Cherenkov Counters (RICH) provide a kaon identification efficiency of $\sim$95% for a pion fake rate of a

few percent, integrated over the momentum range from 3−100 GeV/c. Downstream of the second RICH is a Preshower/Scintillating Pad Detector (PS/SPD), and electromagnetic (ECAL) and hadronic (HCAL) calorimeters. Information from the ECAL/HCAL is used to form the hadronic triggers. Finally, a muon system consisting of five stations is used for triggering on and identifying muons.

To reduce the 40 MHz crossing rate to about 2 kHz for permanent storage, LHCb uses a two-level trigger system. The first level of the trigger, L0, is hardware based and searches for either a large transverse energy cluster ($E_T > 3.6$ GeV) in the calorimeters, or a single high p_T or di-muon pair in the muon stations. Events passing L0 are read out and sent to a large computing farm, where they are analyzed using a software-based trigger. The first level of the software trigger, called HLT1, uses a simplified version of the offline software to apply tighter selections on charged particles based on their p_T and minimal IP to any primary vertex (PV), defined as the location of the reconstructed pp collision(s). The HLT1 trigger relevant for this analysis searches for a single track with IP larger than 125 μm, $p_T > 1.8$ GeV/c, $p > 12.5$ GeV/c, along with other track quality requirements. Events that pass HLT1 are analyzed by a second software level, HLT2, where the event is searched for 2, 3, or 4-particle vertices that are consistent with b-hadron decays. Tracks are required to have $p > 5$ GeV/c, $p_T > 0.5$ GeV/c and IP χ^2 larger than 16 to any PV, where the χ^2 value is obtained assuming the IP is equal to zero. We also demand that at least one track has $p_T > 1.5$ GeV/c, a scalar p_T sum of the track in the vertex exceed 4 GeV/c, and that the corrected mass[2] is between 4 and 7 GeV/c^2. These HLT trigger selections each have an efficiency in the range of 80−90% for events that pass typical offline selections for a large range of B decays. A more detailed description of the LHCb detector can be found in Ref. [13].

Events with large occupancy are known to have intrinsically high backgrounds and to be slow to reconstruct. Therefore such events were suppressed by applying global event cuts (GECs) to hadronically triggered decays. These GECs included a maximum of 3000 VELO clusters, 3000 IT hits, and 10,000 OT hits. In addition, hadron triggers were required to have less than 900 or 450 hits in the SPD, depending on the specific trigger setting.

3 Candidate Reconstruction and Selection

Charged particles likely to come from a b-hadron decay are first identified by requiring that they have a minimum IP χ^2 with respect to any PV of more than 9. We also require a minimum transverse momentum, $p_T > 300$ MeV/c, except for $H_b \to H_c\pi^-\pi^+\pi^-$ decays, where we allow (at most) one track to have $200 < p_T < 300$ MeV/c. Hadrons are identified using RICH information by requiring the difference in log-likelihoods (ΔLL) of the different mass hypotheses to satisfy $\Delta LL(K-\pi) > -5$, $\Delta LL(p-\pi) > -5$ and

[2]The corrected mass is defined as $M_{\rm cor} = \sqrt{M^2 + p_{\rm trans}^2}$, where M is the invariant mass of the 2, 3 or 4-track candidate (assuming the kaon mass for each particle), and $p_{\rm trans}$ is the momentum imbalance transverse to the direction of flight, defined by the vector that joins the primary and secondary vertices.

$\Delta LL(K-\pi) < 12$, for kaons, protons and pions, respectively. These particle hypotheses are not mutually exclusive, however the same track cannot enter more than once in the same decay chain.

Charm particle candidates are reconstructed in the decay modes $D^0 \to K^-\pi^+$, $D^+ \to K^-\pi^+\pi^+$, $D_s^+ \to K^+K^-\pi^+$ and $\Lambda_c^+ \to pK^-\pi^+$. The candidate is associated to one of the PVs in the event based on the smallest IP χ^2 between the charm particle's reconstructed trajectory and all PVs in the event. A number of selection criteria are imposed to reduce backgrounds from both prompt charm with random tracks as well as purely combinatorial background. To reduce the latter, we demand that each candidate is well separated from the associated PV by requiring that its flight distance (FD) projected onto the z-axis is larger than 2 mm, the FD $\chi^2 > 49$[3], and that the distance in the transverse direction (ΔR) is larger than 100 μm. Background from random track combinations is also suppressed by requiring the vertex fit χ^2/ndf< 8, and $p_T > 1.25$ GeV/c (1.5 GeV/c for $D_{(s)}^+$ in $\overline{B}_s^0 \to D_s^+\pi^-$.) To reduce the contribution from prompt charm, we require that the charm particle has a minimal IP larger than 80 μm and IP $\chi^2 > 12.25$ with respect to its associated PV. For $D_s^+ \to K^+K^-\pi^+$, we employ tighter particle identification requirements on the kaons, namely $\Delta LL(K-\pi) > 0$, if the K^+K^- invariant mass is outside a window of ± 20 MeV/c^2 of the ϕ mass [15]. Lastly, we require the reconstructed charm particles masses to be within 25 MeV/c^2 of their known values.

The bachelor pion for $H_b \to H_c\pi^-$ is required to have $p_T > 0.5$ GeV/c, $p > 5.0$ GeV/c and IP $\chi^2 > 16$. For the 3π vertex associated with the $H_b \to H_c\pi^-\pi^+\pi^-$ decays, we apply a selection identical to that for the charm particle candidates, except we only require the p_T of the 3π system to be larger than 1 GeV/c and that the invariant mass is in the range from 0.8 GeV/$c^2 < M(\pi\pi\pi) <$ 3.0 GeV/c^2.

Beauty hadrons are formed by combining a charm particle with either a single pion candidate (for $H_b \to H_c\pi^-$) or a 3π candidate (for $H_b \to H_c\pi^-\pi^+\pi^-$.) The b-hadron is required to have a transverse momentum of at least 1 GeV/c. As with the charm hadron, we require it is well-separated from its associated PV, with FD larger than 2 mm, FD $\chi^2 > 49$ and $\Delta R > 100$ μm. We also make a series of requirements that ensure that the b-hadron candidate is consistent with a particle produced in a proton-proton interaction. We require the candidate to have IP$<$90 μm, IP $\chi^2 < 16$, and that the angle θ between the b-hadron momentum and the vector formed by joining the associated PV and the decay vertex satisfies $\cos\theta > 0.99996$. To ensure a good quality vertex fit, we require a vertex fit χ^2/ndf< 6 (8 for $H_b \to H_c\pi^-$.)

To limit the timing to process high occupancy events, we place requirements on the number of tracks[4] in an event. For $\overline{B}^0 \to D^+\pi^-$ and $\overline{B}_s^0 \to D_s^+\pi^-$, the maximum number of tracks is 180, and for $\Lambda_b^0 \to \Lambda_c^+\pi^-$ and $B^- \to D^0\pi^-$ it is 120. These selections are 99% and 95% efficient, respectively, after the GECs. The $H_b \to H_c\pi^-\pi^+\pi^-$ selection requires fewer than 300 tracks, and thus is essentially 100% efficient after the GECs.

Events are required to pass the triggers described above. This alone does not imply

[3]This is the χ^2 with respect to the FD=0 hypothesis.

[4]Here, tracks refer to charged particles that have segments in both the VELO and the T-stations.

that the signal b-hadron decay was directly responsible for the trigger. We therefore also require that one or more of the signal b-hadron daughters is responsible for triggering the event. We thus explicitly select events that **T**riggered **O**n the **S**ignal decay (**TOS**) at L0, HLT1 and HLT2. For the measurements of excited charm states, where our yields are statistically limited, we also make use of L0-triggers that **T**riggered **I**ndependently of the **S**ignal decay (**TIS**). In this case, the L0 trigger is traced to one or more particles other than those in the signal decay.

Lastly, we note that in $H_b \to H_c\pi^-\pi^+\pi^-$ candidate events, between 4% and 10% have multiple candidates (mostly two) in the same event. In such cases we choose the candidate with the largest transverse momentum. This criterion is estimated to be $(75 \pm 20)\%$ efficient for choosing the correct candidate. For $H_b \to H_c\pi^-$ multiple candidates occur in less than 1% of events, from which we again choose the one with the largest p_T.

3.1 Selection Efficiencies

Selection and trigger efficiencies are estimated using Monte Carlo (MC) simulations. The MC samples are generated with an average number of interactions per crossing equal to 2.5, which is similar to the running conditions for the majority of the 2010 data. The b-hadrons are produced using PYTHIA [16] and decayed using EVTGEN [17]. The $H_b \to H_c\pi^-\pi^+\pi^-$ decays are produced using a cocktail for the $\pi\pi\pi$ system that is $\sim$2/3 $a_1(1260)^- \to \rho^0\pi^-$ and about 1/3 non-resonant $\rho^0\pi^-$. Smaller contributions from $D_1^0(2420)\pi$ and $D_2^{*0}(2460)\pi$ are each included at the 5% level to $B^- \to D^0\pi^-\pi^+\pi^-$ and 2% each for $\overline{B}^0 \to D^+\pi^-\pi^+\pi^-$. For $\Lambda_b^0 \to \Lambda_c^+\pi^-\pi^+\pi^-$, we include contributions from $\Lambda_c(2595)^+$ and $\Lambda_c(2625)^+$, which contribute 9% and 7% to the MC sample. The detector is simulated with GEANT4 [18], and the event samples are subsequently analyzed in the same way as data.

We compute the total kinematic efficiency, $\epsilon_{\rm kin}$ from the MC simulation as the fraction of all events that pass all reconstruction and selection requirements. These selected events are then passed through a software emulation of the L0 trigger, and the HLT software used to select the data, from which we compute the trigger efficiency ($\epsilon_{\rm trig}$). The efficiencies for the decay modes under study are shown in Table 1. Only the relative efficiencies are used to obtain the results in this paper.

4 Reconstructed Signals in Data

The reconstructed invariant mass distributions are shown in Figs. 2 and 3 for the signal and normalization modes, respectively. Unbinned likelihood fits are performed to extract the signal yields, where the likelihood functions are given by the sums of signal and several background components. The signal and background components are shown in the figures. The signal contributions are each described by the sum of two Gaussian shapes with equal means. The relative width and fraction of the wider Gaussian shape with respect to the narrower one are constrained to the values found from MC simulation based on agreement

Table 1: Summary of efficiencies for decay channels under study. Here, $\epsilon_{\rm kin}$ is the total kinematic selection efficiency, $\epsilon_{\rm trig}$ is the trigger efficiency, and $\epsilon_{\rm tot}$ is their product. The uncertainties shown are statistical only.

Decay	$\epsilon_{\rm kin}$ (%)	$\epsilon_{\rm trig}$ (%)	$\epsilon_{\rm tot}$ (%)
$\overline{B}^0 \to D^+\pi^-\pi^+\pi^-$	0.153 ± 0.003	22.6 ± 0.5	0.0347 ± 0.0011
$B^- \to D^0\pi^-\pi^+\pi^-$	0.275 ± 0.007	27.4 ± 0.6	0.0753 ± 0.0019
$\overline{B}^0_s \to D^+_s\pi^-\pi^+\pi^-$	0.137 ± 0.003	24.9 ± 0.7	0.0342 ± 0.0012
$\Lambda^0_b \to \Lambda^+_c\pi^-\pi^+\pi^-$	0.110 ± 0.005	24.0 ± 0.7	0.0264 ± 0.0008
$\overline{B}^0 \to D^+\pi^-$	0.882 ± 0.014	20.8 ± 0.3	0.184 ± 0.004
$B^- \to D^0\pi^-$	1.54 ± 0.02	27.4 ± 0.3	0.421 ± 0.007
$\overline{B}^0_s \to D^+_s\pi^-$	0.868 ± 0.010	23.1 ± 0.2	0.201 ± 0.003
$\Lambda^0_b \to \Lambda^+_c\pi^-$	0.732 ± 0.015	24.7 ± 0.4	0.181 ± 0.004

with data in the large yield signal modes. This constraint is included with a 10-12% uncertainty (mode-dependent), which is the level of agreement found between data and MC simulation. The absolute width of the narrower Gaussian is a free parameter in the fit, since the data shows a slightly worse ($\sim$10%) resolution that MC simulation.

For $\overline{B}^0_s \to D^+_s\pi^-$ and $\overline{B}^0_s \to D^+_s\pi^-\pi^+\pi^-$ decays, there are peaking backgrounds from $\overline{B}^0 \to D^+\pi^-$ and $\overline{B}^0 \to D^+\pi^-\pi^+\pi^-$ just below the B^0_s mass. We therefore fix their core Gaussian widths as well, based on the resolutions found in data for the kinematically similar $\overline{B}^0 \to D^+\pi^-$ and $\overline{B}^0 \to D^+\pi^-\pi^+\pi^-$ decays, scaled by 0.93, which is the ratio of expected widths obtained from MC simulation.

A number of backgrounds contribute to these decays. Below the b-hadron masses there are generally peaking background structures due to partially reconstructed B decays. These decays include $B_{(s)} \to D^*_{(s)}\pi(\pi\pi)$, with a missed photon, π^0 or π^+, as well as $B_{(s)} \to D_{(s)}\rho^-$, where the π^0 is not included in the decay hypothesis. For the $\overline{B}^0 \to D^+\pi^-$ and $B^- \to D^0\pi^-$ decays, the shapes of these backgrounds are taken from dedicated signal MC samples. The double-peaked background shape from partially-reconstructed $D^*\pi$ decays is obtained by fitting the background MC sample to the sum of two Gaussian shapes with different means. The difference in their means is then fixed, while their average is a free parameter in subsequent fits to the data. For $\overline{B}^0 \to D^+\pi^-\pi^+\pi^-$ and $B^- \to D^0\pi^-\pi^+\pi^-$, the shape of the partially-reconstructed $D^*\pi\pi\pi$ background is not as easily derived since the helicity amplitudes are not known. This low mass background is also parametrized using a two-Gaussian model, but we let the parameters float in the fit to the data. For $\overline{B}^0_s \to D^+_s\pi^-$ and $\overline{B}^0_s \to D^+_s\pi^-\pi^+\pi^-$, we obtain the background shape from a large $\overline{B}^0_s \to D^+_s X$ inclusive MC sample. Less is known about the Λ^0_b hadronic decays that would contribute background to the $\Lambda^0_b \to \Lambda^+_c\pi^-$ and $\Lambda^0_b \to \Lambda^+_c\pi^-\pi^+\pi^-$ invariant mass spectra. For $\Lambda^0_b \to \Lambda^+_c\pi^-\pi^+\pi^-$, we see no clear structure due to partially-reconstructed backgrounds. For $\Lambda^0_b \to \Lambda^+_c\pi^-$, there does appear to be structure at about 5430 MeV/c^2,

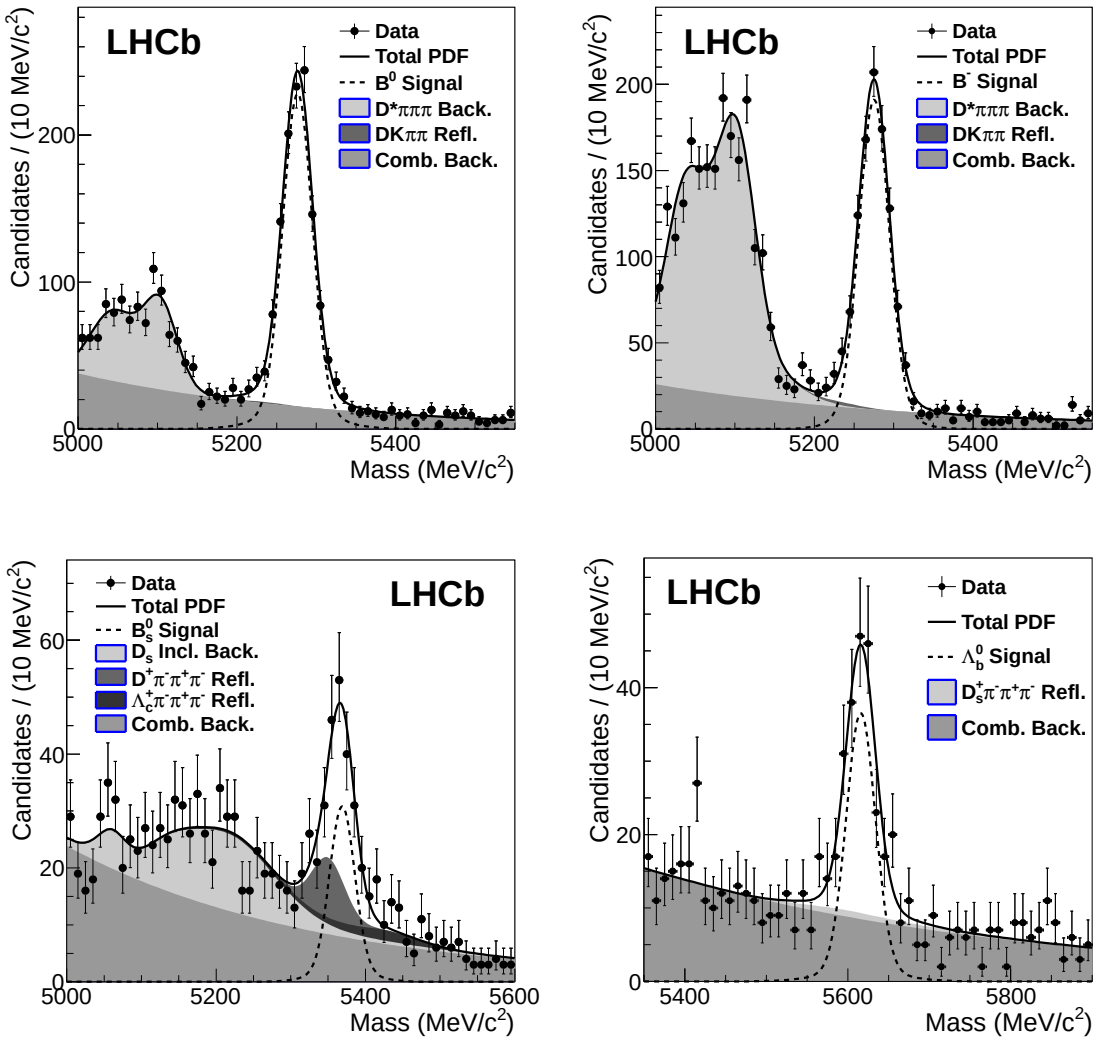

Figure 2: Invariant mass distributions for $\overline{B}^0 \to D^+\pi^-\pi^+\pi^-$ (top left), $B^- \to D^0\pi^-\pi^+\pi^-$ (top right), $\overline{B}^0_s \to D^+_s\pi^-\pi^+\pi^-$ (bottom left), and $\Lambda^0_b \to \Lambda^+_c\pi^-\pi^+\pi^-$ (bottom right). Fits showing the signal and background components are indicated, and are described in the text.

which may be due to $\Lambda^+_c\rho^-$. The enhancement is described by a single Gaussian above the combinatoric background, which, given the limited number of events, provides a good description of this background.

There are also so-called reflection backgrounds, where fully reconstructed signal decays from one b-hadron decay mode produce peaking structures in the invariant mass spectra of other decay modes when one of the daughter particles is misidentified. For $B \to D\pi^-(\pi^+\pi^-)$, there are reflections from $B \to DK^-(\pi^+\pi^-)$ Cabibbo-suppressed decays, where the kaon is misidentified as a pion. Due to the Cabibbo suppression and the

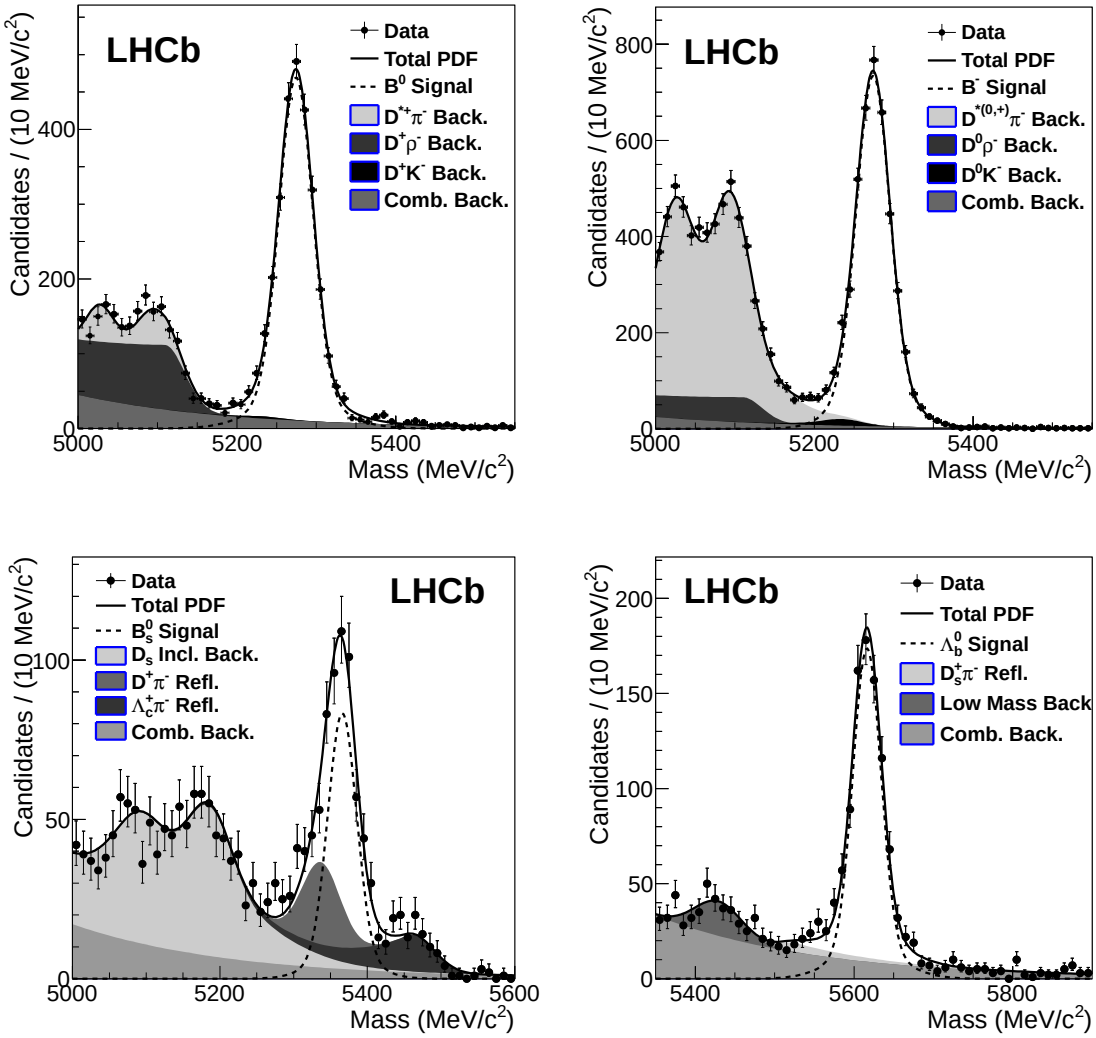

Figure 3: Invariant mass distributions for $\overline{B}^0 \to D^+\pi^-$ (top left), $B^- \to D^0\pi^-$ (top right), $\overline{B}^0_s \to D^+_s\pi^-$ (bottom left), and $\Lambda^0_b \to \Lambda^+_c\pi^-$ (bottom right). Fits showing the signal and background components are indicated, and are described in the text.

excellent RICH performance, their contributions are limited to the 1% level. The shape of this misidentification background is taken from MC simulation and is constrained to be $(1 \pm 1)\%$ of the signal yield.

For the $\overline{B}^0_s \to D^+_s\pi^-$ and $\overline{B}^0_s \to D^+_s\pi^-\pi^+\pi^-$ decays, there are reflection backgrounds from $\overline{B}^0 \to D^+\pi^-$ and $\overline{B}^0 \to D^+\pi^-\pi^+\pi^-$ modes, when either of the π^+ from the D^+ decay is misidentified as a K^+. This cross-feed background is evaluated in two ways. First, we take our $\overline{B}^0 \to D^+\pi^-$ ($\overline{B}^0 \to D^+\pi^-\pi^+\pi^-$) data, which have very loose particle identification (PID) requirements on the pions, and apply the kaon PID selection to them. If either of the two pions pass, and the recomputed $(KK\pi)$ mass is within the D^+_s mass

window, the candidate is counted as a reflection background. Using this technique, we find $(5.3 \pm 0.4)\%$ $[(6.3 \pm 0.6)\%]$ of $\overline{B}^0 \to D^+\pi^-$ $[\overline{B}^0 \to D^+\pi^-\pi^+\pi^-]$ signal decays reflect into the $\overline{B}^0_s \to D^+_s\pi^-$ $[\overline{B}^0_s \to D^+_s\pi^-\pi^+\pi^-]$ signal region. In the second method, we apply a π-faking-K misidentification matrix (in bins of p and p_T), obtained from a D^{*+} data calibration sample to the $\overline{B}^0 \to D^+\pi^-$ (or $\overline{B}^0 \to D^+\pi^-\pi^+\pi^-$) signal MC sample, followed by the D^+_s mass window requirement (after replacing the pion mass with the kaon mass.) The results of this second procedure are $(4.4 \pm 0.3)\%$ for $\overline{B}^0 \to D^+\pi^-$ and $(5.2 \pm 0.4)\%$ for $\overline{B}^0 \to D^+\pi^-\pi^+\pi^-$, both of which are consistent with the first method. We therefore constrain the peaking background from $\overline{B}^0 \to D^+\pi^-$ ($\overline{B}^0 \to D^+\pi^-\pi^+\pi^-$) into $\overline{B}^0_s \to D^+_s\pi^-$ ($\overline{B}^0_s \to D^+_s\pi^-\pi^+\pi^-$) to be $(4.0 \pm 1.5)\%$ ($(5.0 \pm 2.0)\%$), where the Gaussian constraint is conservatively assigned a 40% relative uncertainty. The shape of this peaking background is obtained from MC simulation and is well-described by a single Gaussian of mean 5350 MeV/c^2 and width 30 MeV/c^2. This shape is in good agreement with what is observed in data.

The second reflection background to $\overline{B}^0_s \to D^+_s\pi^-$ ($\overline{B}^0_s \to D^+_s\pi^-\pi^+\pi^-$) is $\Lambda^0_b \to \Lambda^+_c\pi^-$ ($\Lambda^0_b \to \Lambda^+_c\pi^-\pi^+\pi^-$), where the proton from the Λ_c decay is misidentified as a kaon. This is similar to the $\overline{B}^0$ reflection, except here the Λ^0_b yield is significantly smaller, obviating the need for making an explicit $\Delta LL(K-p)$ requirement to reject protons. The Λ^0_b reflection background is evaluated using the first technique as described above leading to reflection rates of $(15 \pm 3)\%$ for $\Lambda^0_b \to \Lambda^+_c\pi^-$ into $\overline{B}^0_s \to D^+_s\pi^-$ and $(20 \pm 4)\%$ for $\Lambda^0_b \to \Lambda^+_c\pi^-\pi^+\pi^-$ into $\overline{B}^0_s \to D^+_s\pi^-\pi^+\pi^-$. We conservatively assign a 20% uncertainty on this rate based on the agreement between data and MC simulation. The asymmetric shape of this background is described by the simulation, which is consistent with the shape observed in data. The combinatorial background is modeled with an exponential distribution. The fits are superimposed on the data in Figs. 2 and 3, and the fitted yields are summarized in Table 2.

The ratios of branching ratios are given by:

$$\frac{\mathcal{B}(H_b \to H_c\pi^-\pi^+\pi^-)}{\mathcal{B}(H_b \to H_c\pi^-)} = \frac{Y^{\rm sig}/\epsilon^{\rm sig}_{\rm tot}}{Y^{\rm norm}/\epsilon^{\rm norm}_{\rm tot}}$$

where the Y factors are the observed yields in the signal and normalization modes, and $\epsilon_{\rm tot}$ are the total selection efficiencies.

5 Systematic Uncertainties

Several sources contribute uncertainty to the measured ratios of branching fractions. Because we are measuring ratios of branching fractions, most, but not all of the potential systematics cancel. Here, we discuss only the non-cancelling uncertainties. With regard to the reconstruction of the $H_b \to H_c\pi^-\pi^+\pi^-$ and $H_b \to H_c\pi^-$ decays, the former has two additional pions which need to pass our selections, and the 3π system needs to pass the various vertex-related selection criteria. The track reconstruction efficiency and uncertainty are evaluated by measuring the ratio of fully reconstructed J/ψ's to all J/ψ's

Table 2: Summary of yields for the branching fraction computation. Uncertainties are statistical only.

Decay	Yield	Decay	Yield
$\overline{B}^0 \to D^+\pi^-\pi^+\pi^-$	1150 ± 43	$\overline{B}^0 \to D^+\pi^-$	2745 ± 66
$B^- \to D^0\pi^-\pi^+\pi^-$	950 ± 41	$B^- \to D^0\pi^-$	4244 ± 90
$\overline{B}^0_s \to D^+_s\pi^-\pi^+\pi^-$	138 ± 23	$\overline{B}^0_s \to D^+_s\pi^-$	434 ± 32
$\Lambda^0_b \to \Lambda^+_c\pi^-\pi^+\pi^-$	174 ± 18	$\Lambda^0_b \to \Lambda^+_c\pi^-$	853 ± 36

obtained from an inclusive single muon trigger, where only one of the muons is required to be reconstructed. After reweighting the efficiencies to match the kinematics of the signal tracks, the uncertainty is found to be 2% per track, which leads to a 4% uncertainty in the branching fraction ratios. The IP resolution in data is about 20% worse than in the simulation, leading to (i) a larger efficiency for tracks to pass the IP-related cuts (as well as larger background), and (ii) a lower efficiency to pass the vertex χ^2 selections, for data relative to the value predicted by simulation. The first of these is studied by reducing the IP χ^2 requirement in simulation by 20%, and the second by smearing the vertex χ^2 distribution in simulation until it agrees with data. The combined correction is found to be 1.02 ± 0.03.

Another potential source of systematic uncertainty is related to the production and decay model for producing the $H_c\pi\pi\pi$ final state. We have considered that the p_T spectrum of the pions in the 3π system may be different between simulation and data. To estimate the uncertainty, we reweight the MC simulation to replicate the momentum spectrum of the lowest momentum pion (amongst the pions in the 3π vertex.) We find that the total efficiency using the reweighted spectra agrees with the unweighted spectra to within 3%. We have also investigated the effect of differences in the p_T spectra of the charm particle, and find at most a 1% difference. Our candidate selection is limited to the mass region $M(\pi\pi\pi) < 3$ GeV/c^2. Given that the phase space population approaches zero as $M(\pi\pi\pi) \to 3.5$ GeV/c^2 (*i.e.*, $M_B - M_D$) and that the simulation reasonably reproduces the $\pi^-\pi^+\pi^-$ mass spectrum, we use the simulation to assess the fraction of the $\pi\pi\pi$ mass spectrum beyond 3 GeV/c^2. We find the fraction of events above 3 GeV/c^2 is $(3.5-4.5)\%$ for the decay modes under study. We apply a correction of 1.04 ± 0.02, where we have assigned half the correction as an estimate of the uncertainty. In total, the correction for production and decay models is 1.04 ± 0.04.

As discussed in Sec. 3, we choose only one candidate per event. The efficiency of this selection is estimated by comparing the signal yield in multiple-candidate events before and after applying the best candidate selection. The selection is estimated to be $(75\pm20)\%$ efficient. In the $H_b \to H_c\pi^-\pi^+\pi^-$ the multiple candidate rate varies from 4% to 10%, so we have corrections that vary from 1.01 to 1.03. For $H_b \to H_c\pi^-$, this effect is negligible. The corrections for each mode are given in Table 3.

For the trigger efficiency, we rely on signal MC simulations to emulate the online trigger. The stability of the relative trigger efficiency was checked by reweighting the

b-hadron p_T spectra for both the signal and normalization modes, and re-evaluating the trigger efficiency ratios. We find maximum differences of 2% for L0, 1% for HLT1 and 1% for HLT2, (2.4% total) which we assign as a systematic uncertainty.

Fitting systematics are evaluated by varying the background shapes and assumptions about the signal parameterization for both the $H_b \to H_c\pi^-\pi^+\pi^-$ and $H_b \to H_c\pi^-$ modes and re-measuring the yield ratios. For the combinatorial background, using first and second order polynomials leads to a 3% uncertainty on the relative yield. Reflection background uncertainties are negligible, except for $\overline{B}^0_s \to D^+_s\pi^-\pi^+\pi^-$ and $\overline{B}^0_s \to D^+_s\pi^-$, where we find deviations as large as 5% when varying the central value of the constraints on the $\overline{B}^0 \to D^+\pi^-\pi^+\pi^-$ and $\overline{B}^0 \to D^+\pi^-$ reflections by ± 1 standard deviation. We have checked our sensitivity to the signal model by varying the constraints on the width ratio and core Gaussian area fraction by one standard deviation (2%). We also include a systematic uncertainty of 1% for neglecting the small radiative tail in the fit, which is estimated by comparing the yields between our double Gaussian signal model and the sum of a Gaussian and Crystal Ball [20] line shape. Taken together, we assign a 4% uncertainty to the relative yields. For the $\overline{B}^0_s$ branching fraction ratio, the total fitting uncertainty is 6.4%.

Another difference between the $H_b \to H_c\pi^-$ and $H_b \to H_c\pi^-\pi^+\pi^-$ selection is the upper limit on the number of tracks. The efficiencies of the lower track multiplicity requirements can be evaluated using the samples with higher track multiplicity requirements. Using this technique, we find corrections of 0.95 ± 0.01 for the B^- and Λ^0_b branching fraction ratios, and 0.99 ± 0.01 for the $\overline{B}^0$ and $\overline{B}^0_s$ branching fraction ratios.

We have also studied the PID efficiency uncertainty using a D^{*+} calibration sample in data. Since the PID requirements are either common to the signal and normalization modes, or in the case of the bachelor pion(s), the selection is very loose, the uncertainty is small and we estimate a correction of 1.01 ± 0.01. We have also considered possible background from $H_b \to H_c D^-_s$ which results in a correction of 0.99 ± 0.01.

All of our MC samples have a comparable number of events, from which we incur 3-4% uncertainty in the efficiency ratio determinations. The full set of systematic uncertainties and corrections are shown in Table 3. In total, the systematic uncertainty is $\sim$9%, with correction factors that range from 1.01 to 1.07.

Table 3: Summary of corrections and systematic uncertainties to the ratio of branching fractions $\mathcal{B}(H_b \to H_c\pi^-\pi^+\pi^-)/\mathcal{B}(H_b \to H_c\pi^-)$.

Source	central value ± syst. error			
	$\overline{B}^0$	B^-	$\overline{B}^0_s$	Λ_b
Track Reconstruction	1.00 ± 0.04			
IP/Vertex Resolution	1.02 ± 0.03			
Production/Decay Model	1.04 ± 0.04			
Best Cand. Selection	1.02 ± 0.02	1.01 ± 0.01	1.02 ± 0.02	1.03 ± 0.02
Trigger Efficiency	1.00 ± 0.02			
Fitting	1.00 ± 0.04	1.00 ± 0.04	1.00 ± 0.06	1.00 ± 0.04
Cut on #Tracks	0.99 ± 0.01	0.95 ± 0.01	0.99 ± 0.01	0.95 ± 0.01
PID	1.01 ± 0.01			
$H_cD_s^+$ background	0.99 ± 0.01			
MC Statistics	1.00 ± 0.04	1.00 ± 0.03	1.00 ± 0.04	1.00 ± 0.04
Total Correction	1.07	1.01	1.07	1.03
Total Systematic (%)	8.8	8.4	10.1	9.2

6 Results for $H_b \to H_c\pi^-\pi^+\pi^-$

The results for the ratios of branching ratios are

$$\begin{aligned}
\frac{\mathcal{B}(\overline{B}^0 \to D^+\pi^-\pi^+\pi^-)}{\mathcal{B}(\overline{B}^0 \to D^+\pi^-)} &= 2.38 \pm 0.11 \pm 0.21 \\
\frac{\mathcal{B}(B^- \to D^0\pi^-\pi^+\pi^-)}{\mathcal{B}(B^- \to D^0\pi^-)} &= 1.27 \pm 0.06 \pm 0.11 \\
\frac{\mathcal{B}(\overline{B}^0_s \to D^+_s\pi^-\pi^+\pi^-)}{\mathcal{B}(\overline{B}^0_s \to D^+_s\pi^-)} &= 2.01 \pm 0.37 \pm 0.20 \\
\frac{\mathcal{B}(\Lambda^0_b \to \Lambda^+_c\pi^-\pi^+\pi^-)}{\mathcal{B}(\Lambda^0_b \to \Lambda^+_c\pi^-)} &= 1.43 \pm 0.16 \pm 0.13,
\end{aligned} \tag{1}$$

where the first uncertainty is statistical and the second is systematic. These measurements are all substantially more precise than the current world average values. Naively, one might have expected the four branching fraction ratios to be nearly equal. The observed differences may be explained in terms of the contributing Feynman diagrams. From Fig. 1, we see that the primary contribution to $\overline{B}^0 \to D^+\pi^-(\pi^+\pi^-)$ and $\overline{B}^0_s \to D^+_s\pi^-(\pi^+\pi^-)$ is from a single decay diagram, an external tree diagram. On the other hand the $B^- \to D^0\pi^-(\pi^+\pi^-)$ and $\Lambda^0_b \to \Lambda^+_c\pi^-(\pi^+\pi^-)$ amplitudes receive contributions from both external and color-suppressed tree diagrams. This would suggest that the interference tends to be more constructive in $B^- \to D^0\pi^-$ and $\Lambda^0_b \to \Lambda^+_c\pi^-$ than in $B^- \to D^0\pi^-\pi^+\pi^-$ and $\Lambda^0_b \to \Lambda^+_c\pi^-\pi^+\pi^-$ respectively. The role of the various contributing topological amplitudes

and the strong phases in $B \to D\pi$ is discussed in the literature [12]. In general we see the branching fractions for the $H_c\pi\pi\pi$ final states are at least as large or even twice as large as the single-π bachelor states.

7 Kinematic Distributions and Mass Spectra in the $\pi^-\pi^+\pi^-$ System

Since we rely on MC simulation to estimate signal efficiencies, we now compare a few distributions between signal MC simulation and data. The higher signal yield $\overline{B}^0 \to D^+\pi^-$ and $\overline{B}^0 \to D^+\pi^-\pi^+\pi^-$ decay modes are used, and for each we perform a sideband subtraction, where the signal region includes candidates within 50 MeV/c^2 of the B^0 mass, (m_{B^0}) [15], and the sidebands $60 < |M - m_{B^0}| < 110$ MeV/c^2. For both data and simulation, we require events to pass any L0 trigger, and signal candidates must satisfy the HLT1 and HLT2 triggers described in Sec. 2. Clearly, two of the most important quantities used in our candidate selection are the p_T and IP of the daughters from the D^+ and the recoiling pion(s). Figure 4 compares the p_T and IP distributions of the D^+ daughters in data to those from signal MC simulation. Figure 5 shows the corresponding comparisons for the recoiling pion(s) in the respective B decay. Overall, the agreement between data and MC simulation is very good.

It is also interesting to examine the $\pi^-\pi^+\pi^-$ invariant mass spectra for the four signal decay modes. Here, we use the sPlot method [19] to obtain the underlying signal spectra, based on the event-by-event b-hadron mass signal and background probabilities. The $\pi^-\pi^+\pi^-$ mass spectra are shown in Fig. 6, along with signal MC shapes that are normalized to the same yield as data. We also show several resonant contributions: $D_1(2420)^+$ (2%), $D_1(2420)^0$ and $D_2^*(2460)^0$ (14% in total), $\Lambda_c(2595)^+$ and $\Lambda_c(2625)^+$ (9% total), and Σ_c^0 and Σ_c^{++} (12% total), where the quantities in parentheses are the normalizations relative to the total (see Sec. 8.) A prominent structure at low mass, consistent with the $a_1(1260)^-$ is evident for all decay modes, along with a long tail extending to 3 GeV/c^2. In all cases, the 3π mass spectrum appears shifted toward lower mass as compared to the MC simulation. The simulated value for the $a_1(1260)^-$ mass is 1230 MeV/c^2, which is equal to the central value given in the PDG [15] of (1230 ± 40) MeV/c^2. Besides having a large uncertainty, the mass as obtained by experiment may be process-dependent, so it is difficult to draw any definitive conclusion from this shift. Since both the reconstruction and trigger efficiency are flat through this mass region, this small shift in mass does not introduce any significant systematic uncertainty in the branching fraction measurement.

We have also looked at the di-pion invariant masses within the 3π system, shown for $\overline{B}^0 \to D^+\pi^-\pi^+\pi^-$(a,b) and $B^- \to D^0\pi^-\pi^+\pi^-$(c,d) in Fig. 7. Contributions from the narrow excited charm states, which are discussed in Sec. 8, are excluded. In all cases, in the low $M(\pi^-\pi^+\pi^-)$ mass region, we see a dominant $\rho^0\pi^-$ contribution, consistent with the $a_1(1260)^-$ resonance. In the higher $M(\pi\pi\pi)$ regions there appears to be an additional resonant structure, consistent with the $f_2(1270)$ state, in addition to the ρ^0 contribution. Similar spectra are found for $\overline{B}_s^0 \to D_s^+\pi^-\pi^+\pi^-$ and $\Lambda_b^0 \to \Lambda_c^+\pi^-\pi^+\pi^-$ (not shown.)

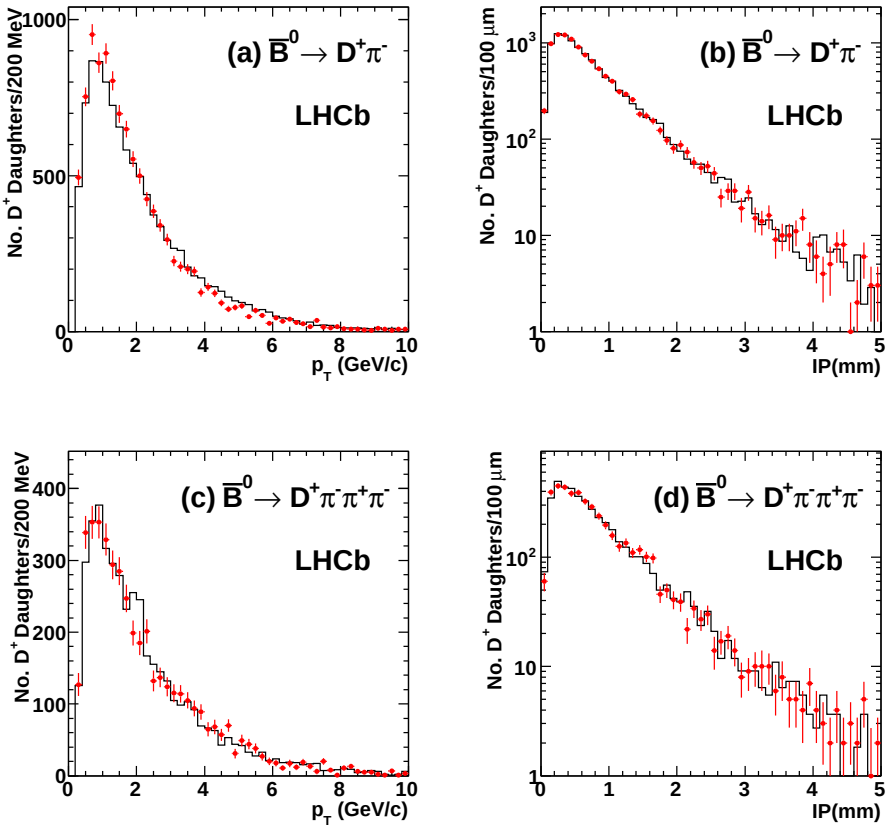

Figure 4: Comparisons of the p_T and IP spectra for the daughters from the D^+ in $\overline{B}^0 \to D^+\pi^-$ [(a) and (b)], and from the D^+ in $\overline{B}^0 \to D^+\pi^-\pi^+\pi^-$ [(c) and (d)]; Points with error bars are data and the solid lines are simulation.

The $f_2(1270)$ has been previously seen in $\overline{B}^0 \to D^{*+}\pi^-\pi^+\pi^-$ [21]. The like-sign di-pion invariant mass spectra do not show any resonant features.

8 Contributions from Excited Charm Hadrons

Within the $H_b \to H_c\pi^-\pi^+\pi^-$ final state, we search for $D_1(2420)$, $D_2^*(2460)$, $\Lambda_c(2595)^+$, $\Lambda_c(2625)^+$ and $\Sigma_c^{0,++}$, which may decay to D or Λ_c^+ with an accompanying $\pi^\pm$ or $\pi\pi$ pair. To search for $H_c^* \to H_c\pi^+\pi^-$ intermediate states, we select events in the b-hadron signal region (± 60 MeV/c^2 around the nominal mass) and compute the invariant mass difference $\Delta M_{\pi\pi} \equiv M(H_c\pi^+\pi^-) - M(H_c)$ (two combinations per b-hadron candidate.) For the $\Lambda_b^0 \to \Sigma_c^{0,++}\pi^\pm\pi^-$, $\Sigma_c^{0,++} \to \Lambda_c^+\pi^\pm$, we use $\Delta M_\pi \equiv M(H_c\pi^\pm) - M(H_c)$ in a similar way (one (two) Σ_c^{++} (Σ_c^0) candidates per Λ_b^0 decay.) We also have looked in the upper mass sidebands, and the $\Delta M_{\pi\pi}$ and ΔM_π distributions are consistent with a smooth background shape with no signal component. We look at all data, irrespective of trigger,

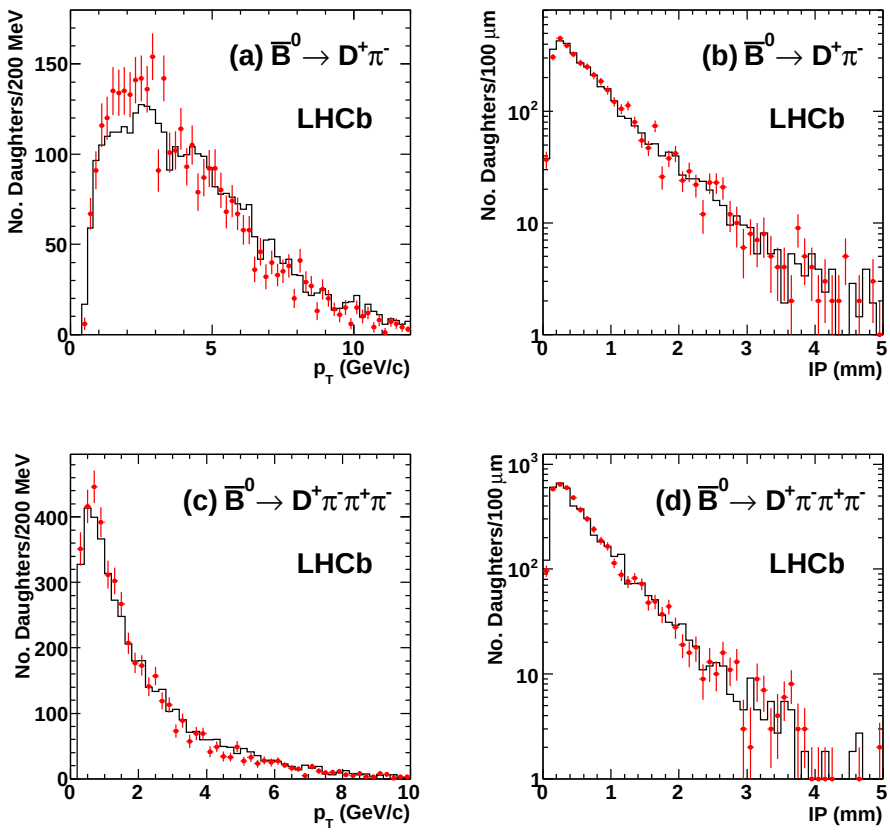

Figure 5: Comparisons of the p_T and IP spectra for the bachelor pion in $\overline{B}^0 \to D^+\pi^-$ [(a) and (b)], and for the 3 pions in $\overline{B}^0 \to D^+\pi^-\pi^+\pi^-$ [(c) and (d)]. Points with error bars are data and the solid lines are simulation.

to establish signal significances, but for the branching fraction measurement, we use the same trigger requirements described in Sec. 7. We choose only one candidate per event using the same criteria as discussed previously. We normalize the rates to the respective inclusive $H_b \to H_c\pi^-\pi^+\pi^-$ decay, using the same trigger selection as above. We show only the $\Delta M_{\pi\pi}$ and ΔM_π distributions after the specified trigger, since the distributions before the trigger are quite similar, except they typically have 25−30% larger yields than the ones shown.

The $\Delta M_{\pi\pi}$ distributions for $\overline{B}^0$ and B^+ are shown in Fig. 8 and the ΔM_π for Λ_b^0 are shown in Fig. 9. For B_s^0, the size of the data sample is insufficient to observe the excited D_s states in these hadronic decays.

Signal yields are determined using unbinned extended maximum likelihood fits. Starting with $\overline{B}^0$ (Fig. 8(a)), we see an excess at $\Delta M_{\pi\pi} \sim 560$ MeV/c^2, consistent with the $D_1(2420)^+$. We fit the distribution to the sum of a signal Breit-Wigner shape convoluted with a Gaussian resolution, and an exponential background shape. The full width is fixed to 25 MeV/c^2 [15] and the mass resolution is set to 7.5 MeV/c^2 based on simulation. The

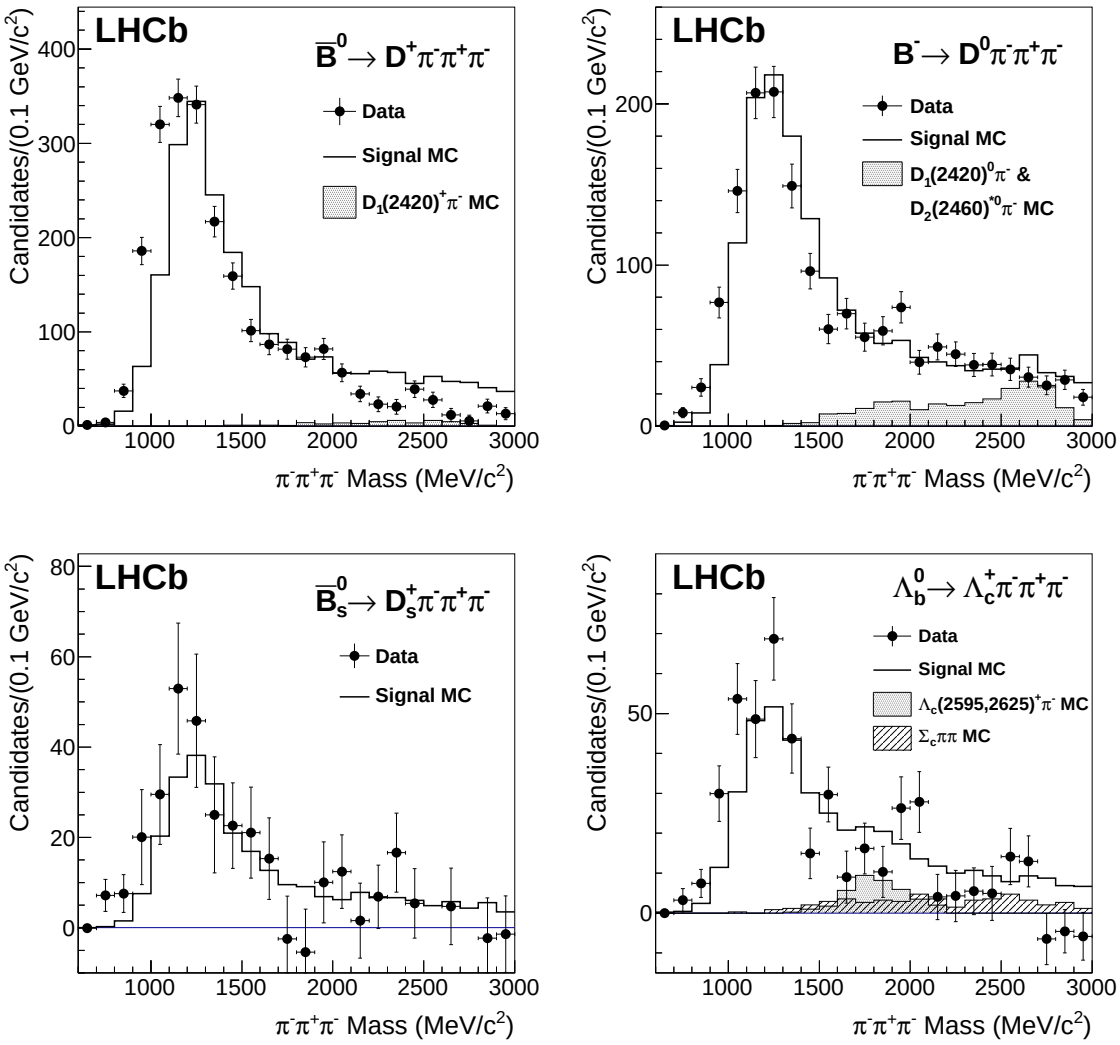

Figure 6: Invariant mass of the 3π system in $\overline{B}^0 \to D^+\pi^-\pi^+\pi^-$ (top left), $B^- \to D^0\pi^-\pi^+\pi^-$ (top right), $\overline{B}_s^0 \to D_s^+\pi^-\pi^+\pi^-$ (bottom left) and $\Lambda_b^0 \to \Lambda_c^+\pi^-\pi^+\pi^-$ (bottom right) decays. The data are the points with error bars and the simulations are the solid lines and shaded regions.

fitted yield is 33 ± 8 events and the fitted mean is (562 ± 4) MeV/c^2, consistent with the expected value. If the width is allowed to float, we find $(22.7 \pm 8.0(\text{stat}))$ MeV/c^2, also in agreement with the world average. Prior to applying the specific trigger selection, we find 40 ± 9 signal events, corresponding to a statistical significance of 6.8 standard deviations (for one degree of freedom) as determined from the difference in log-likelihoods, $\sqrt{-2\Delta LL}$, where the difference is taken between the signal yield taken as a free parameter and fixed to zero.

The $\Delta M_{\pi\pi}$ distributions for B^- displayed in Fig. 8(b) show not only the $D_1(2420)^0$,

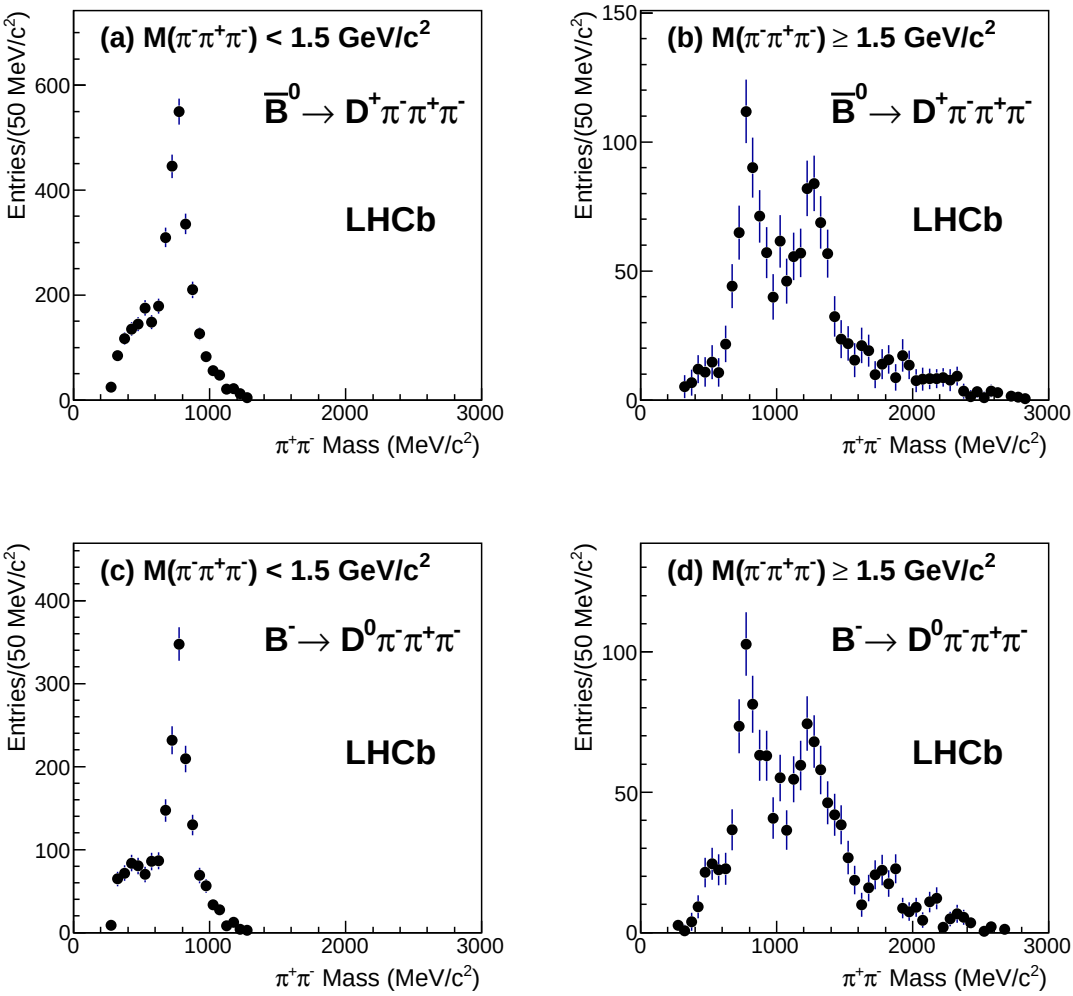

Figure 7: $\pi^+\pi^-$ invariant mass (2 combinations per $\overline{B}^0$ candidate) in the 3π system for $\overline{B}^0 \to D^+\pi^-\pi^+\pi^-$ when (a) $M(\pi^-\pi^+\pi^-) < 1.5$ GeV/c^2 and (b) $M(\pi^-\pi^+\pi^-) \geq 1.5$ GeV/c^2. The corresponding plots for $B^- \to D^0\pi^-\pi^+\pi^-$ are shown in (c) and (d).

but also a shoulder at $\sim$600 MeV/c^2, consistent with the $D_2^*(2460)^0$. Hence, we allow for both $D_1(2420)^0$ and $D_2^*(2460)^0$ signal components, and fix their full widths to the PDG values [15] of 20.4 MeV/c^2 and 42.9 MeV/c^2, respectively. The means and yields are left as free parameters in the fit. The fitted $D_1(2420)^0$ and $D_2^*(2460)^0$ yields are 124 ± 14 and 49 ± 12, with masses that are consistent with the expected values. The respective signal yields before the trigger requirement are 165 ± 17 and 63 ± 15 events, with corresponding statistical significances of 10.5 and 5.5 standard deviations for the $D_1(2420)^0$ and $D_2^*(2460)^0$, respectively. These B^0 and B^- decays have also been observed by Belle [22].

We have also measured the relative fractions of $D_1(2420)^0$ and $D_2^*(2460)^0$ that do or

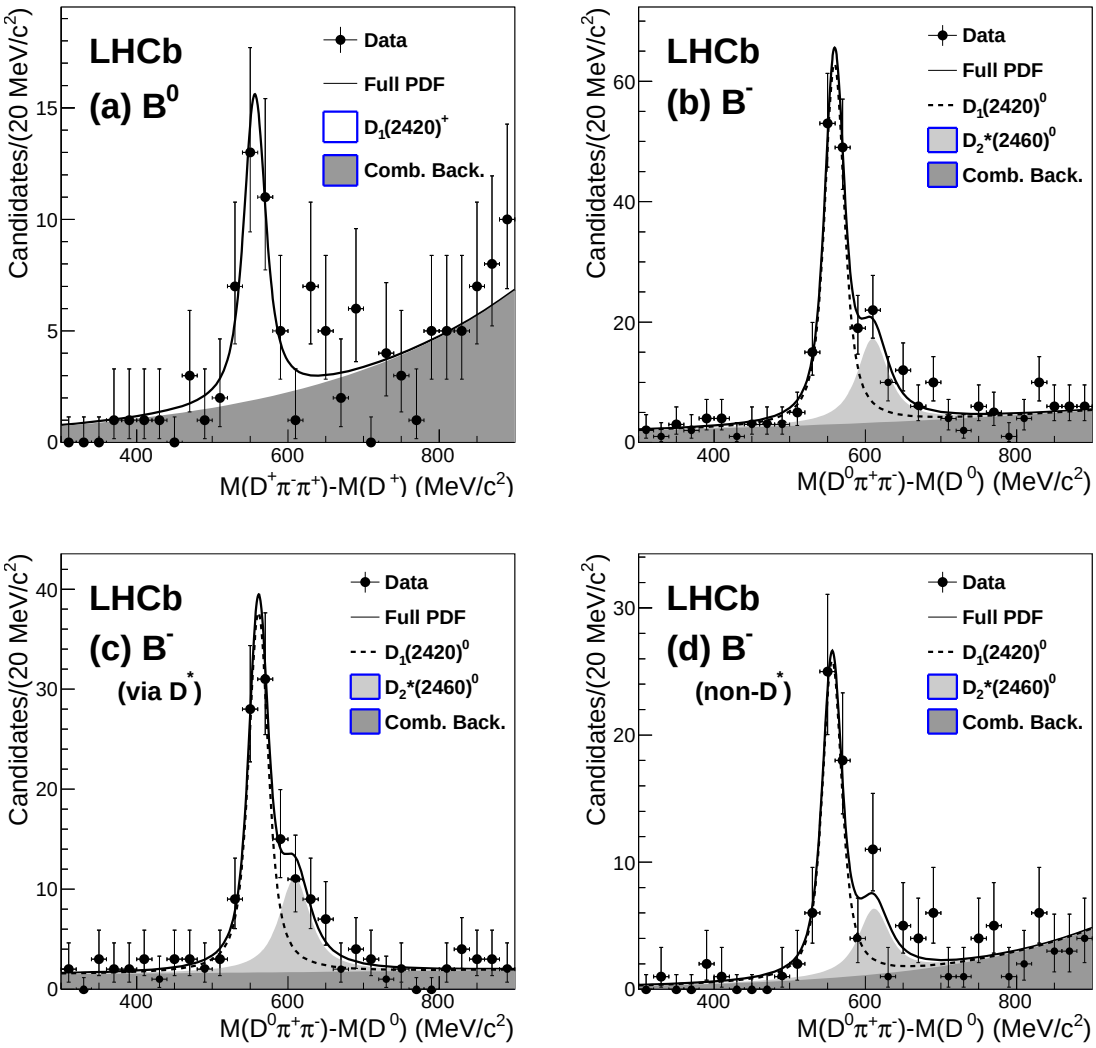

Figure 8: Invariant mass difference $M(D\pi^-\pi^+) - M(D)$, for (a) $\overline{B}^0 \to D^+\pi^-\pi^+\pi^-$ signal candidates, (b) $B^- \to D^0\pi^-\pi^+\pi^-$ signal candidates, (c) $B^- \to D^0\pi^-\pi^+\pi^-$ through a D^{*+} intermediate state, and (d) $B^- \to D^0\pi^-\pi^+\pi^-$ not through a D^{*+} intermediate state. The signal components are the white region (and lightly shaded regions for $B^- \to D^0\pi^-\pi^+\pi^-$), and the background component is the darker shaded region.

do not decay through D^{*+} by taking the subset of candidates with $M(D^0\pi^+) - M(D^0) \leq 150\,\mathrm{MeV}/c^2$ or $M(D^0\pi^+) - M(D^0) > 150\,\mathrm{MeV}/c^2$, respectively. The corresponding $\Delta M_{\pi\pi}$ distributions are shown in Fig. 8(c) and Fig. 8(d). A fit is made to the data as discussed previously, and the yields are summarized in Table 4.

For Λ_b^0 (see Fig. 9(a)), we find two well-separated peaks in the $\Delta M_{\pi\pi}$ distribution, one at $\sim$307 MeV/c^2, and a second at $\sim$340 MeV/c^2, consistent with the expected values for the $\Lambda_c(2595)^+$ and $\Lambda_c(2625)^+$, respectively. The full width of the $\Lambda_c(2595)^+$ is fixed to the

PDG value of 3.6 MeV/c^2, and the mass resolution for each peak is fixed to 2.0 MeV/c^2, as determined from simulation. The fitted signal yields are 9.7 ± 3.5 and 9.3 ± 3.2 for the $\Lambda_c(2595)^+$ and $\Lambda_c(2625)^+$, respectively. Before the trigger, we find signal yields of 10.6 ± 3.8 for $\Lambda_c(2595)^+$ and 15.7 ± 4.1 for $\Lambda_c(2625)^+$, corresponding to statistical significances of 4.3 and 6.6 standard deviations. Thus we have evidence for $\Lambda_b^0 \to \Lambda_c(2595)^+\pi^-$ and observation of $\Lambda_b^0 \to \Lambda_c(2625)^+\pi^-$. The systematic uncertainties do not change this conclusion. These decays have also been reported by CDF [23], but are not yet published. The fitted $\Delta M_{\pi\pi}$ values of (306.7 ± 1.1) MeV/c^2 and (341.7 ± 0.6) MeV/c^2, for the $\Lambda_c(2625)^+$ and $\Lambda_c(2625)^+$, respectively, are consistent with the known mass differences [15] for these excited states.

We also observe the decays $\Lambda_b^0 \to \Sigma_c^{0,++}\pi^\mp\pi^-$, with $\Sigma_c^0 \to \Lambda_c^+\pi^-$ or $\Sigma_c^{++} \to \Lambda_c^+\pi^+$. The ΔM_π distributions are shown in Fig. 9(b-d) for both Σ_c^0 and Σ_c^{++} candidates, Σ_c^0 candidates only (c), and (d) Σ_c^{++} candidates only. The data are fit to the sum of a Breit-Wigner shape convolved with a Gaussian resolution function and a smooth threshold function. The full width is fixed to 2.2 MeV/c^2 [15] in all cases, and the ΔM_π resolution is fixed to 1 MeV/c^2 based on simulation. The combined Σ_c^0 and Σ_c^{++} signal has a statistical significance of 6.0 standard deviations. The Σ_c^0 and Σ_c^{++} signals have statistical significances of 4.9 and 3.5, respectively. These decays have also been seen by CDF [23].

Table 4 summarizes the yields for the various excited charm states for both the full data sample and after the trigger selection as well as the yields in the normalizing modes (after trigger selection.)

Table 4: Summary of yields for the signal and normalization modes. Below D_1 and D_2^* refer to the $D_1(2420)$ and $D_2^*(2460)$ mesons, respectively.

Decay	$H_c^*\pi(\pi)$ Signal Yields		$H_c\pi^-\pi^+\pi^-$
	All	Trig. Sel	Trig. Sel
$\overline{B}^0 \to D_1^+\pi^-,\ D_1^+ \to D^+\pi^-\pi^+$	41 ± 8	33 ± 7	1741 ± 55
$B^- \to D_1^0\pi^-,\ D_1^0 \to D^0\pi^-\pi^+$	165 ± 17	126 ± 14	1386 ± 51
$B^- \to D_1^0\pi^-,\ D_1^0 \to D^{*+}\pi^-$	111 ± 14	75 ± 12	1386 ± 51
$B^- \to D_1^0\pi^-,\ D_1^0 \to D^0\pi^-\pi^+,\ \text{non}-D^*$	57 ± 10	52 ± 9	1386 ± 51
$B^- \to D_2^{*0}\pi^-,\ D_2^{*0} \to D^0\pi^-\pi^+$	66 ± 15	49 ± 12	1386 ± 51
$B^- \to D_2^{*0}\pi^-,\ D_2^{*0} \to D^{*+}\pi^-$	46 ± 12	34 ± 10	1386 ± 51
$B^- \to D_2^{*0}\pi^-,\ D_2^{*0} \to D^0\pi^-\pi^+,\ \text{non}-D^*$	23 ± 9	18 ± 8	1386 ± 51
$\Lambda_b^0 \to \Lambda_c(2595)^+\pi^-$	10.6 ± 3.8	9.7 ± 3.5	312 ± 23
$\Lambda_b^0 \to \Lambda_c(2625)^+\pi^-$	15.7 ± 4.1	9.3 ± 3.2	312 ± 23
$\Lambda_b^0 \to \Sigma_c^{0,++}\pi^\mp\pi^-$	29.3 ± 7.0	24.9 ± 6.2	312 ± 23
$\Lambda_b^0 \to \Sigma_c^0\pi^-\pi^+$	19.6 ± 5.7	16.2 ± 5.0	312 ± 23
$\Lambda_b^0 \to \Sigma_c^{++}\pi^-\pi^-$	10.1 ± 4.0	9.3 ± 3.7	312 ± 23

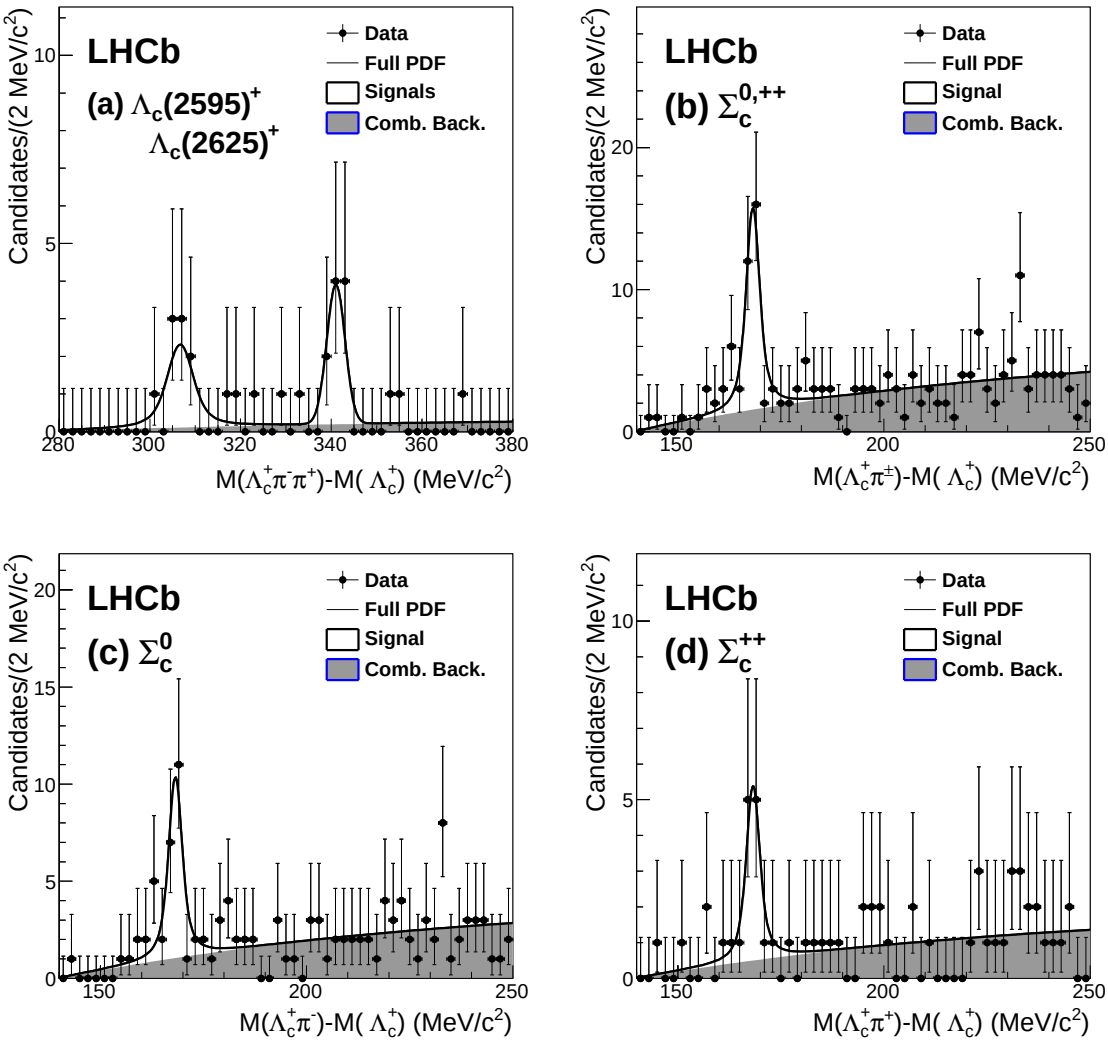

Figure 9: Intermediate resonances contributing to the $\Lambda_b^0 \to \Lambda_c^+\pi^-\pi^+\pi^-$ decay. Shown are distributions for (a) $M(\Lambda_c^+\pi^-\pi^+) - M(\Lambda_c^+)$, with $\Lambda_c(2595)^+$ and $\Lambda_c(2625)^+$ contributions, (b) $M(\Lambda_c^+\pi^\pm) - M(\Lambda_c^+)$ (3 combinations per Λ_b^0 candidate) (c) $M(\Lambda_c^+\pi^-) - M(\Lambda_c^+)$ (2 combinations per Λ_b^0 candidate), and (d) $M(\Lambda_c^+\pi^+) - M(\Lambda_c^+)$ (1 combination per Λ_b^0 candidate), showing the intermediate Σ_c states. The line is a fit as described in the text, and the shaded region is the fitted background.

The branching ratios for these modes are computed using:

$$\frac{\mathcal{B}(H_b \to H_c^*\pi(\pi)) \times \mathcal{B}(H_c^* \to H_c\pi(\pi))}{\mathcal{B}(H_b \to H_c\pi^-\pi^+\pi^-)} = \frac{N_{\rm signal}}{N_{\rm norm}} \left(\epsilon_{\rm sel}^{\rm rel} \times \epsilon_{\rm trig|sel}^{\rm rel}\right)^{-1} \tag{2}$$

where H_c^* refers to one of the observed excited charm states, $N_{\rm signal}$ and $N_{\rm norm}$ are the number of reconstructed decays in the signal and normalization modes after the trigger

requirement, $\epsilon^{\rm rel}_{\rm sel}$ is the reconstruction and selection efficiency relative to the normalization mode, and $\epsilon^{\rm rel}_{\rm trig|sel}$ is the relative trigger efficiency. All efficiencies are given for the mass region 0.8 GeV/$c^2 < M(\pi^-\pi^+\pi^-) <$ 3 GeV/c^2.

The relative reconstruction, selection and trigger efficiencies, shown in Table 5, are evaluated using MC simulations. The $D_1(2420)^0$ and $D_2^*(2460)^0$ are each assumed to decay 70% through $D^{*+}\pi^- \to D^0\pi^+\pi^-$ and 30% non-resonant $D^0\pi^+\pi^-$. The $D_1(2420)^+$ is taken to be 100% non-resonant $D^+\pi^-\pi^+$. The $\Lambda_c(2595)^+$ decay is simulated as 36% $\Sigma_c^0\pi^+$, 36% $\Sigma_c^{++}\pi^-$ and 28% non-resonant $\Lambda_c^+\pi^-\pi^+$. The $\Lambda_c(2625)^+$ decay is assumed to be 100% non-resonant $\Lambda_c^+\pi^-\pi^+$. The $\Sigma_c(2544)$ baryons are simulated non-resonant in phase space.

The relative efficiencies agree qualitatively with our expectations based on the kinematics and proximity to threshold for these excited charm states. The differences in the relative efficiency between the pairs of excited charm states for a given b-hadron species are negligible compared to the uncertainty from our limited MC event sample, and we use the average relative efficiency for each pair of decays.

Table 5: Summary of the relative reconstruction and selection efficiencies ($\epsilon^{\rm rel}_{\rm sel}$) and trigger efficiencies ($\epsilon^{\rm rel}_{\rm trig|sel}$) for the excited charm hadron intermediate states with respect to the inclusive $H_c\pi^-\pi^+\pi^-$ final states. Below D_1 and D_2^* refer to $D_1(2420)$ and $D_2^*(2460)$, respectively. The uncertainties shown are statistical only.

Decay	$\epsilon^{\rm rel}_{\rm sel}$ (%)	$\epsilon^{\rm rel}_{\rm trig|sel}$ (%)	$\epsilon^{\rm rel}_{\rm total}$ (%)
$\overline{B}^0 \to D_1^+\pi^-$	0.83 ± 0.06	1.05 ± 0.09	0.87 ± 0.10
$B^- \to (D_1^0,\ D_2^{*0})\pi^-$	0.70 ± 0.04	1.24 ± 0.07	0.86 ± 0.07
$B^- \to (D_1^0,\ D_2^{*0})\pi^-$(via D^*)	0.66 ± 0.05	1.29 ± 0.08	0.84 ± 0.08
$B^- \to (D_1^0,\ D_2^{*0})\pi^-$(non$-D^*$)	0.78 ± 0.06	1.15 ± 0.10	0.91 ± 0.11
$\Lambda_b^0 \to (\Lambda_c(2595),\ \Lambda_c(2625)^+)\pi^-$	0.52 ± 0.03	1.30 ± 0.07	0.67 ± 0.06
$\Lambda_b^0 \to \Sigma_c^{0,++}\pi\pi,\ \Sigma_c^{0,++} \to \Lambda_c^+\pi^\mp$	0.67 ± 0.05	1.10 ± 0.13	0.75 ± 0.10

The dominant sources of systematic uncertainty are the limited MC sample sizes and the fit model. Starting with the $\overline{B}^0$, the uncertainty due to limited MC statistics is 11%. For the fit model, the largest source of uncertainty is from a possible $D_2^*(2460)^+\pi^-,\ D_2^*(2460)^+ \to D^+\pi^-\pi^+$ contribution. If this contribution is included in the fit using a Breit-Wigner shape with mean and width taken from the PDG [15], the returned signal yield is 0^{+7}_{-0}. If we assume isospin symmetry, and constrain this fraction (relative to $D_1(2420)$) to be (40 ± 11)%, the ratio found for the B^- decay, the fitted $\overline{B}^0 \to D_1(2420)^+\pi^-,\ D_1(2420)^+ \to D^+\pi^-\pi^+$ signal yield is 26 ± 6 events. We take this as a one-sided uncertainty of $^{+0\%}_{-21\%}$. Sensitivity to the background shape is estimated

by using a second order polynomial for the background (3%). The $\overline{B}^0$ mass sidebands, which have a $D_1(2420)^+$ fitted yield of 2^{+3}_{-2} events from which we conservatively assign as a one-sided systematic uncertainty of $^{+0\%}_{-6\%}$. For the signal decays, 4% of events have $M(\pi^-\pi^+\pi^-) > 3$ GeV/c^2, whereas for the $D_1(2420)^+$, we find a negligible fraction fail this requirement. We therefore apply a correction of 0.96 ± 0.02, where we have taken 50% uncertainty on the correction as the systematic error. The systematic uncertainty on the yield in the $\overline{B}^0 \to D^+\pi^-\pi^+\pi^-$ normalizing mode is 3%. We thus arrive at a total systematic error on the $\overline{B}^0$ branching fraction ratio of $^{+12}_{-25}$%.

For the B^-, we have a similar set of uncertainties. They are as follows: MC sample size (8%), background model (1%, 2%), $D_1(2420)^0$ width (2%, 4%), $D_2^*(2460)^0$ width (1%, 3%), where the two uncertainties are for the ($D_1(2420)^0$, $D_2^*(2460)^0$) intermediate states. We have not accounted for interference, and have assumed it is negligible compared to other uncertainties. A factor of 0.98 ± 0.01 is applied to correct for the fraction of events with $M(\pi^-\pi^+\pi^-) > 3$ GeV/c^2. Including a 3% uncertainty on the $B^- \to D^0\pi^-\pi^+\pi^-$ yield, we find total systematic errors of 9% and 10% for the $D_1(2420)^0$ and $D_2^*(2460)^0$ intermediate states, respectively. For the D^* sub-decays, the total systematic uncertainties are 10% and 11% for $B^- \to D_1(2420)^0\pi^-$, $D_1(2420)^0 \to D^{*+}\pi^-$ and $B^- \to D_2^*(2460)^0\pi^-$, $D_2^*(2460)^0 \to D^{*+}\pi^-$, respectively. For final states not through D^*, we find a total systematic uncertainty of 13% for both intermediate states. In all cases, the dominant systematic uncertainty is the limited number of MC events.

For the Λ_b^0 branching fraction ratios, we attribute uncertainty to limited MC sample sizes (8%), the $\Lambda_c^+(2595)$ width ($^{+9\%}_{-5\%}$), $\Lambda_b^0 \to \Lambda_c^+\pi^-\pi^+\pi^-$ signal yield (3%), and apply a correction of 0.96 ± 0.02 for the ratio of yields with $M(\pi^-\pi^+\pi^-) > 3$ GeV/c^2. In total, the systematic uncertainties on the $\Lambda_c^+(2595)^+$ and $\Lambda_c(2625)^+$ partial branching fractions are $^{+13\%}_{-10\%}$ and $\pm 10\%$, respectively.

For the $\Sigma_c^{0,++}$ intermediate states, the systematic uncertainties include 14% from finite MC statistics, and 4% from the $\Sigma_c^{0,++}$ width. For the $\Sigma_c^{0,++}$ simulation, 10% of decays have $M(\pi^-\pi^+\pi^-) > 3$ GeV/c^2, compared to 4% for the normalizing mode. We therefore apply a correction of 1.06 ± 0.03 to the ratio of branching fractions. All other uncertainties are negligible in comparison. We thus arrive at a total systematic uncertainty of 16%.

The final partial branching fractions are

$$\frac{\mathcal{B}(\overline{B}^0 \to D_1^- \pi^+,\ D_1^- \to D^+\pi^-\pi^+)}{\overline{B}^0 \to D^+\pi^-\pi^+\pi^-} = (2.1 \pm 0.5^{+0.3}_{-0.5})\%$$
$$\frac{\mathcal{B}(B^- \to D_1^0 \pi^+,\ D_1^0 \to D^0\pi^-\pi^+)}{B^- \to D^0\pi^-\pi^+\pi^-} = (10.3 \pm 1.5 \pm 0.9)\%$$
$$\frac{\mathcal{B}(B^- \to D_1^0 \pi^+,\ D_1^0 \to D^{*+}\pi^-)}{B^- \to D^0\pi^-\pi^+\pi^-} = (9.3 \pm 1.6 \pm 0.9)\%$$
$$\frac{\mathcal{B}(B^- \to D_1^0 \pi^+,\ D_1^0 \to D^0\pi^-\pi^+)_{\mathrm{non}-D^*}}{B^- \to D^0\pi^-\pi^+\pi^-} = (4.0 \pm 0.7 \pm 0.5)\%$$
$$\frac{\mathcal{B}(B^- \to D_2^{*0} \pi^+,\ D_2^{*0} \to D^0\pi^-\pi^+)}{B^- \to D^0\pi^-\pi^+\pi^-} = (4.0 \pm 1.0 \pm 0.4)\%$$
$$\frac{\mathcal{B}(B^- \to D_2^{*0} \pi^+,\ D_2^{*0} \to D^{*+}\pi^-)}{B^- \to D^0\pi^-\pi^+\pi^-} = (3.9 \pm 1.2 \pm 0.4)\%$$
$$\frac{\mathcal{B}(B^- \to D_2^{*0} \pi^+,\ D_2^{*0} \to D^0\pi^-\pi^+)_{\mathrm{non}-D^*}}{B^- \to D^0\pi^-\pi^+\pi^-} = (1.4 \pm 0.6 \pm 0.2)\%$$
$$< 3.0\% \text{ at } 90\% \text{ C.L.}$$
$$\frac{\mathcal{B}(\Lambda_b^0 \to \Lambda_c(2595)^+\pi^+,\ \Lambda_c(2595)^+ \to \Lambda_c^+\pi^-\pi^+)}{\Lambda_b^0 \to \Lambda_c^+\pi^-\pi^+\pi^-} = (4.4 \pm 1.7^{+0.6}_{-0.4})\%$$
$$\frac{\mathcal{B}(\Lambda_b^0 \to \Lambda_c(2625)^+\pi^+,\ \Lambda_c(2625)^+ \to \Lambda_c^+\pi^-\pi^+)}{\Lambda_b^0 \to \Lambda_c^+\pi^-\pi^+\pi^-} = (4.3 \pm 1.5 \pm 0.4)\%$$
$$\frac{\mathcal{B}(\Lambda_b^0 \to \Sigma_c^{0,++}\pi^\mp\pi^-,\ \Sigma_c^{0,++} \to \Lambda_c^+\pi^\mp)}{\Lambda_b^0 \to \Lambda_c^+\pi^-\pi^+\pi^-} = (11.4 \pm 3.1 \pm 1.8)\%$$
$$\frac{\mathcal{B}(\Lambda_b^0 \to \Sigma_c^0\pi^+\pi^-,\ \Sigma_c^0 \to \Lambda_c^+\pi^-)}{\Lambda_b^0 \to \Lambda_c^+\pi^-\pi^+\pi^-} = (7.4 \pm 2.4 \pm 1.2)\%$$
$$\frac{\mathcal{B}(\Lambda_b^0 \to \Sigma_c^{++}\pi^-\pi^-,\ \Sigma_c^{++} \to \Lambda_c^+\pi^+)}{\Lambda_b^0 \to \Lambda_c^+\pi^-\pi^+\pi^-} = (4.2 \pm 1.8 \pm 0.7)\%,$$

where the first uncertainties are statistical and the second are systematic. For the modes with D^{*+}, we include a factor $\mathcal{B}(D^{*+} \to D^0\pi^+) = (0.677 \pm 0.005)$ [15] to account for unobserved D^{*+} decays. The first four and the sixth of these decays have been previously measured by Belle [22] with comparable precision. To compare our results to those absolute branching fractions, we multiply them by the relative $\overline{B}^0$ [B^-] branching fractions in Eq. 1, and then in turn by $\mathcal{B}(\overline{B}^0 \to D^+\pi^-) = (2.68 \pm 0.13) \times 10^{-3}$ [$\mathcal{B}(B^- \to D^0\pi^-) = (4.84 \pm 0.15) \times 10^{-3}$.] The resulting absolute branching fractions are

$$\mathcal{B}(\overline{B}^0 \to D_1(2420)^-\pi^+,\ D_1(2420)^- \to D^+\pi^-\pi^+) = (1.3 \pm 0.3^{+0.2}_{-0.3}) \times 10^{-4}$$
$$\mathcal{B}(B^- \to D_1(2420)^0\pi^+,\ D_1(2420)^0 \to D^0\pi^-\pi^+) = (6.3 \pm 0.9 \pm 0.9) \times 10^{-4}$$
$$\mathcal{B}(B^- \to D_1(2420)^0\pi^+,\ D_1(2420)^0 \to D^{*+}\pi^-) = (5.8 \pm 1.0 \pm 0.9) \times 10^{-4}$$
$$\mathcal{B}(B^- \to D_1(2420)^0\pi^+,\ D_1(2420)^0 \to D^0\pi^+\pi^-)_{\mathrm{non}-D^*} = (2.5 \pm 0.4 \pm 0.4) \times 10^{-4}$$
$$\mathcal{B}(B^- \to D_2^*(2460)^0\pi^+,\ D_2^*(2460)^0 \to D^{*+}\pi^-) = (2.5 \pm 0.7 \pm 0.4) \times 10^{-4}$$

where the uncertainties are statistical and total systematic, respectively. The corresponding values obtained by Belle are: $(0.89^{+0.23}_{-0.35}) \times 10^{-4}$, $(6.5^{+1.1}_{-1.2}) \times 10^{-4}$, $(6.8 \pm 1.5) \times 10^{-4}$, $(1.9^{+0.5}_{-0.6}) \times 10^{-4}$, and $(1.8 \pm 0.5) \times 10^{-4}$ [15, 22]. Our results are consistent with, and of comparable precision to, those measurements.

Preliminary results on the $\Lambda_b^0 \to \Lambda_c^+(2595)^+\pi^-$, $\Lambda_b^0 \to \Lambda_c^+(2625)^+\pi^-$ and $\Lambda_b^0 \to \Sigma_c^{0,++}\pi^\mp\pi^-$ decays have been reported by CDF [23]. Our values are consistent with these (unpublished) results.

9 Summary

In summary, we have measured the branching fractions for $H_b \to H_c\pi^-\pi^+\pi^-$ decays relative to $H_b \to H_c\pi^-$. The ratio of branching fractions are measured to be

$$\frac{\mathcal{B}(\overline{B}^0 \to D^+\pi^-\pi^+\pi^-)}{\mathcal{B}(\overline{B}^0 \to D^+\pi^-)} = 2.38 \pm 0.11 \pm 0.21$$
$$\frac{\mathcal{B}(B^- \to D^0\pi^-\pi^+\pi^-)}{\mathcal{B}(B^- \to D^0\pi^-)} = 1.27 \pm 0.06 \pm 0.11$$
$$\frac{\mathcal{B}(\overline{B}_s^0 \to D_s^+\pi^-\pi^+\pi^-)}{\mathcal{B}(\overline{B}_s^0 \to D_s^+\pi^-)} = 2.01 \pm 0.37 \pm 0.20$$
$$\frac{\mathcal{B}(\Lambda_b^0 \to \Lambda_c^+\pi^-\pi^+\pi^-)}{\mathcal{B}(\Lambda_b^0 \to \Lambda_c^+\pi^-)} = 1.43 \pm 0.16 \pm 0.13.$$

At low 3π mass, these decays appear to be dominated by the $a_1(1260)$ resonance. We have also measured several partial decay rates through excited charm states. The yields of $H_b \to H_c\pi^-\pi^+\pi^-$ relative to $H_b \to H_c\pi^-$ are in the range of 20−40%. If the relative rates in the Cabibbo-suppressed decays, such as $\overline{B}_s^0 \to D_s^\pm K^\mp\pi^\pm\pi^\mp$ and $B^- \to DK^-\pi^+\pi^-$ relative to $\overline{B}_s^0 \to D_s^\pm K^\mp$ and $B^- \to DK^-$, respectively, are comparable, they could be useful for measuring the weak phase γ.

Acknowledgments

We express our gratitude to our colleagues in the CERN accelerator departments for the excellent performance of the LHC. We thank the technical and administrative staff at CERN and at the LHCb institutes, and acknowledge support from the National Agencies: CAPES, CNPq, FAPERJ and FINEP (Brazil); CERN; NSFC (China); CNRS/IN2P3 (France); BMBF, DFG, HGF and MPG (Germany); SFI (Ireland); INFN (Italy); FOM and NWO (Netherlands); SCSR (Poland); ANCS (Romania); MinES of Russia and Rosatom (Russia); MICINN, XuntaGal and GENCAT (Spain); SNSF and SER (Switzerland); NAS Ukraine (Ukraine); STFC (United Kingdom); NSF (USA). We also acknowledge the support received from the ERC under FP7 and the Region Auvergne.

References

[1] N. Cabibbo, Phys. Rev. Lett. **10**, 531 (1963); M. Kobayashi and T. Maskawa, Prog. Theor. Phys. **49**, 652 (1973).

[2] E. Eichten and B. R. Hill, Phys. Lett. **B234**, 511 (1990); N. Isgur and M. B. Wise, Phys.Lett. **B232**, 113 (1989); H. Georgi, Phys. Lett. **B240**, 447 (1990); E. Eichten and B. R. Hill, Phys. Lett. **B243**, 427 (1990); B. Grinstein, Nucl. Phys. **B339**, 253 (1990).

[3] I. Dunietz, Phys. Lett. **B270**, 75 (1991); I. Dunietz, Z. Phys. **C56**, 129 (1992); D. Atwood, G. Eilam, M. Gronau, and A. Soni, Phys. Lett. **B341**, 372 (1995); D. Atwood, I. Dunietz and A. Soni, Phys. Rev. Lett. **78**, 3257 (1997).

[4] M. Gronau and D. London, Phys. Lett. **B253**, 483 (1991); M. Gronau and D. Tyler, Phys. Lett. **B265**, 172 (1991).

[5] A. Giri, Y. Grossman, A. Soffer and J. Zupan, Phys. Rev. **D68** 054018 (2003).

[6] R. Aleksan, I. Dunietz, and B. Kayser, Z. Phys. **C54**, 653 (1992).

[7] I. Dunietz, Phys. Rev. **D52**, 3048 (1995).

[8] C. S. Kim and S. Oh, Eur. Phys. J. **C21**, 495 (2001).

[9] M. Gronau, Phys. Lett. **B557**, 198-206 (2003).

[10] *Measurement of* Δm_s *in the Decay* $B_s^0 \to D_s^-((K^-K^+\pi^-)(3)\pi$, [LHCb Collaboration], LHCb-CONF-2011-005 (2011).

[11] L. Wolfenstein, Phys. Rev. Lett. **51**, 1945 (1983).

[12] C.-W. Chiang and J. Rosner, Phys. Rev. **F67**, 074013 (2003); C. S. Kim *et al* , Phys. Lett **B621**, 259-268 (2004).

[13] A. A. Alves Jr. *et al.* [LHCb Collaboration], JINST 3, S08005 (2008).

[14] M. Williams *et. al.*, LHCb Public Document, LHCb-PUB-2011-002.

[15] K. Nakamura *et al.*, J. Phys. **G37**, 075021 (2010).

[16] T. Sjöstrand, S. Mrenna and P. Skands, JHEP 0605, 026 (2006).

[17] D. J. Lange, Nucl. Instrum. Meth. **A462**, 152 (2001).

[18] S. Agostinelli *et al.* [GEANT4 Collaboration], Nucl. Instrum. Meth. **A506**, 250 (2003).

[19] M. Pivk and F. Le Diberder, Nucl Instrum. Meth **A555**, 356 (2005).

[20] T. Skwarnicki, *A study of the radiative cascade transitions between the Upsilon-prime and Upsilon resonances.* PhD thesis, Institute of Nuclear Physics, Krakow, 1986. DESY-F31-86-02.

[21] D. Monorchio, *Study of the properties of the a_1 meson produced in the $B \to D^{*-} a_1^+$ at the BABAR Experiment*, PhD thesis, Universita Degli Studi Di Napoli, 2005.

[22] K. Abe *et al.* [Belle Collaboration] Phys. Rev. Lett. **94**, 221805 (2005); Phys. Rev. **D69**, 112002 (2004).

[23] P. Azzurri *et al.* [CDF Collaboration], in *Proceedings of Lepton Photon 2009 Conference*, Hamburg, Germany, 17-22 Aug. 2009, p 434, edited by T. Behnke and J. Mnich [arXiv:0912.4380].